RESEARCH ARTICLE | NOVEMBER 12 2024

Report on laser-induced fluorescence transitions relevant for the microelectronics industry and sustainability applications ⓕ⊘

V. S. Santosh K. Kondeti ✉ ⓘ ; Shurik Yatom ⓘ ; Ivan Romadanov ⓘ ; Yevgeny Raitses ⓘ ; Leonid Dorf ⓘ ; Andrei Khomenko ⓘ

Check for updates

View Online

Export Citation
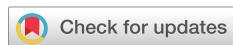
Articles You May Be Interested In

Space and phase resolved ion energy and angular distributions in single- and dual-frequency capacitively coupled plasmas

J. Vac. Sci. Technol. A (October 2013)

Microstructures and microelectronics

Physics Today (November 1979)

Concepts in competitive microelectronics manufacturing

J. Vac. Sci. Technol. B (July 1994)

Report on laser-induced fluorescence transitions relevant for the microelectronics industry and sustainability applications ⓕ

V. S. Santosh K. Kondeti,[1,a)] ⓘ Shurik Yatom,[1] ⓘ Ivan Romadanov,[1] ⓘ Yevgeny Raitses,[1] ⓘ Leonid Dorf,[2] ⓘ and Andrei Khomenko[2] ⓘ

AFFILIATIONS

[1]Princeton Plasma Physics Laboratory, Princeton, New Jersey
[2]Applied Materials, Santa Clara, California

a)Electronic mail: vkondeti@pppl.gov

ABSTRACT

A wide variety of feed gases are used to generate low-temperature plasmas for the microelectronics and sustainability applications. These plasmas often have a complex combination of reactive and nonreactive species which may have spatial and temporal variations in density, temperature, and energy. Accurate knowledge of these parameters and their variations is critically important for understanding and advancing these applications through validated and predictive modeling and the design of relevant devices. Laser-induced fluorescence (LIF) provides both spatial and temporally resolved information about the plasma-produced radicals, ions, and metastables. However, the use of this powerful diagnostic tool requires the knowledge of optical transitions including excitation and fluorescence wavelengths which may not be available or scattered through a huge literature domain. In this paper, we collected, analyzed, and compiled the available transitions for laser-induced fluorescence for more than 160 chemical species relevant to the microelectronics industry and the sustainability applications. A list of species with overlapping LIF excitations and fluorescence wavelengths have been identified. This summary is intended to serve as a data reference for LIF transitions and should be updated in the future.

I. INTRODUCTION

According to Moore's law, the number of transistors on a chip exponentially increase every year.[1–4] The semiconductor industry has been able to keep up with this law by the use of the low-temperature plasma based processes to perform operations such as etching, deposition, or cleaning. The microelectronics industry widely uses plasma-based deposition techniques such as sputtering, plasma-enhanced chemical vapor deposition, oxidation, and planarization.[5] Film and material removal techniques such as etching, photo resist stripping, and cleaning[5] also involve plasma-material interactions. The underlying materials science and the plasma-surface interactions are not completely understood, which poses a significant challenge to develop new tools for the industry. The fabrication of microelectronics in the present era requires sub-nm precision accuracy to enable technologies such as the 3 and the 2 nm nodes.[6] Modern microelectronics industry uses processes such as

atomic layer etching (ALE), atomic layer deposition (ALD), area selective deposition, and high aspect ratio processing to achieve such precision.[7–12] Achieving such precision without damage to the underlying material layer will require meticulous control over the ion energy (or velocity) distribution function (IEDF/IVDF), the fluxes of ions and radicals, and the chemical composition near the material surface.[13,14]

Since their inception, the standard diameter of the silicon wafers used in the microelectronics industry has been increasing to enhance the throughput and reduce the operational cost. Starting from a wafer diameter of 12.5 mm in the year 1957, the industry currently uses a size of 300 mm and proposes to use a size of 450 mm in the future.[15] This increase in wafer size necessitates larger plasma chambers. Radio frequency capacitively coupled plasmas are known for generating large-scale self-organized patterns, leading to spatial nonuniformities that become particularly critical in larger chambers.[16] Etching and deposition occurs on the

silicon wafer surface and it is essential to know the chemical and plasma properties close to the wafer surface. The control over the processes occurring on the wafer surface can be achieved by understanding the chemical stoichiometry close to the wafer surface.[17] The measurement of spatial variation in the properties of the radicals, ions, and metastable species will help in determining the operational parameters that generate a spatially uniform plasma.

Material processing is often controlled by using a pulsed plasma with a duty cycle that allows for periodic intervals where ions or radicals are acting on the material. Volatile products from the material surface are removed during the plasma-off phase. Ions are accelerated toward the material surface by applying a bias voltage on the material surface. By varying the duty cycle of the pulsed plasma, a reproducible high aspect ratio anisotropic etching can be achieved.[13,14] The measurement of the temporal variation of the radicals, ions, and metastable species in a pulsed plasma will validate the simulation models, which are widely used in the microelectronics industry.

The emergence of alternative materials with unique properties such as a single atomic layer or thin films, two-dimensional materials, materials with controlled defects, and nanocrystal assemblies, the semiconductor industry is entering a new post-silicon era.[18] These materials include group III and IV materials, MoS_2, WSe_2, graphene, TiO_2, VO_2, $SmNiO_2$, and others.[19,20] The post-silicon era materials are of interest for quantum computing, quantum electronics, and quantum photonics.[21]

Similar to low-pressure plasmas used in the microelectronics industry, atmospheric pressure plasmas which are widely used for sustainability applications, can also involve a complex chemistry.[6,22,23] These plasmas are used for a wide variety of existing and emerging applications such as plasma medicine,[24] plasma agriculture,[25] plasma synthesis of nanomaterials,[26] plasma catalysis,[27,28] thermal plasmas for welding, cutting and spraying,[29] plasma-assisted combustion,[30] environmental applications,[31,32] pollution control,[33,34] additive manufacturing,[35] and others. These plasmas operate at atmospheric pressure (1 atm) and do not require vacuum hardware to generate the plasma. All these applications require the interaction of plasmas with solids and liquids.[36,37]

While the plasmas used in the microelectronics industry can be tens of cms in dimensions, the plasmas used in sustainability applications vary in size from microplasmas (micrometers to millimeters size)[38] to large volume reactors (several centimeters).[39] Microplasmas have large gradients in the density of ions, electrons, and radical species over a dimension of a mm. Large-volume reactors can result in a spatially nonuniform discharge. To avoid forming filamentary discharges, the atmospheric pressure plasmas are often generated using pulsed voltage waveforms with a duty cycle. So, the plasma is on only for a fraction of the time. Similar to the use of pulsed plasmas for the processing of microelectronics, it results in an intermittent plasma with a temporal variation of the density of electrons, ions, and radicals generated by the plasma.

The predictive design capabilities of the plasma sources used for the microelectronics and sustainability applications can be developed by the comprehensive modeling of the plasma reactors involving hybrid fluid simulations. Modeling is often plagued by the lack of the chemical kinetics information and the experimental data to validate the simulation results. Measurement of the spatial

and temporal variations in the IEDF/IVDF, ion/radical/metastable density distributions, and gas temperatures can inform and improve the predictive capabilities of the simulations. Non-intrusive optical diagnostic techniques such as optical emission spectroscopy and absorption spectroscopy are line-of-sight integrated techniques and obtaining spatially resolved information requires the assumption of a spatial profile.

A laser-based technique such as laser-induced fluorescence can resolve both the spatial and temporal information, while being nonintrusive. Being a resonant laser-based technique, it can detect species even if there is no detectable optical emission from the plasma, in addition to when there is optical emission from the plasma. The LIF transitions for various species such as ions, atoms, and molecules are spread over different scientific papers from various fields. It is often not straightforward to find the different species that can be detected by LIF and the various reported transitions previously reported for a particular species. In this work, we reviewed the basic principles of LIF and the different types of LIF applicable for the microelectronics industry and the sustainability applications. We compiled a LIF reference database with the available LIF transitions that will enable the measurement and detection of the various plasma-produced ions, radicals, and metastables that are relevant for the microelectronics and sustainability applications. We describe the principle, the required instrumentation, calibration, and the applications of LIF in Sec. II. Section III provides the compilation of the LIF transitions and we summarize in Sec. IV.

II. LASER INDUCED FLUORESCENCE

A. Introduction and principle

Laser-induced fluorescence can provide both spatial and temporal measurements of the plasma-produced neutral, ionic, and metastable species. In LIF, laser irradiation resonantly excites the plasma-generated species to a higher electronic state. The excited species emit fluorescence upon relaxation to a lower level. This fluorescence intensity can be used to quantify the species density and the velocity distribution functions.[40–48] When the wavelength required for a resonant transition in LIF falls in the vacuum ultraviolet (VUV) region that is readily absorbed by the ambient air and water vapor, a two-photon excitation scheme is used and the technique is called two-photon absorption laser-induced fluorescence (TALIF). In this method, the energy required for exciting to the upper level is provided by two photons. A schematic of the excitation schemes for LIF and TALIF is shown in Fig. 1(a).

LIF has been used for measuring relative/absolute densities of neutral radical species,[41] velocity distribution functions (VDFs),[49] and rotational temperatures of molecules.[50] Densities as low as $10^8 \, cm^{-3}$ have been successfully measured by LIF when using sensitive modern optical sensors such as a photomultiplier tube (PMT) or an intensified charge-coupled device (iCCD) camera.[51] The spatial resolution of LIF can be as low as $10 \, \mu m$ depending on the laser beam size and the optics used. Absolute densities of neutral radicals can be obtained through calibration of the fluorescence signal. Rayleigh scattering from a known concentration of air coupled with a multi-level model is typically used for obtaining absolute densities for one-photon LIF schemes. Fluorescence from the two-photon excitation of a known concentration of a neutral
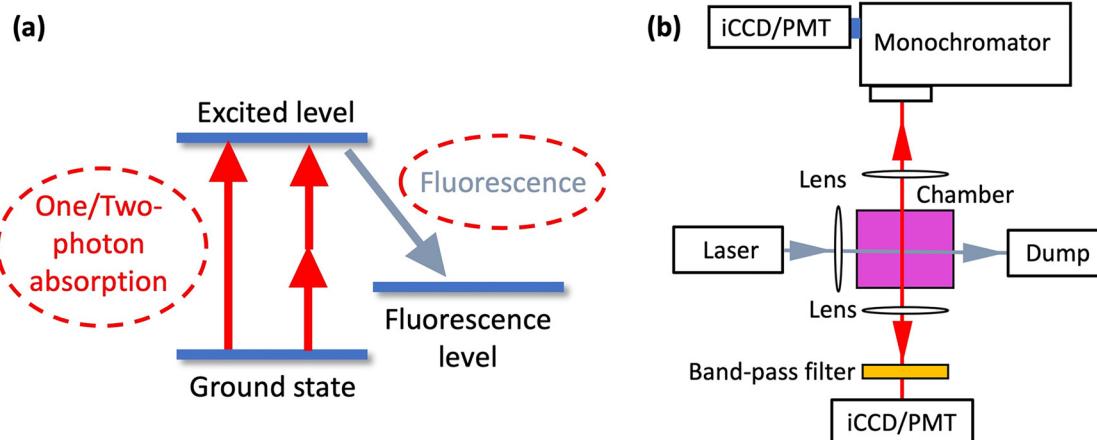
FIG. 1. (a) Transitions schematic and (b) experimental schematic of laser-induced fluorescence.

gas is used for the calibration of TALIF schemes. Details of the calibration methods have been summarized in Sec. II C. For obtaining absolute densities, the laser energy in the LIF measurements is maintained in the linear regime, i.e., when the LIF intensity is proportional to the laser energy. This ensures that the ground state density does not get depleted by the laser beam and the laser energy is spent in the excitation from the lower level to the higher level rather than from the stimulated emission from the higher level to the lower level. Fully saturated laser induced fluorescence has also been used for detecting species using LIF. In the fully saturated LIF regime, a high laser energy is used that ensures that the stimulated emission dominates over the spontaneous emission and the collisional quenching of the excited state.[52,53] Furthermore, saturation will broaden the LIF absorption line profiles and modify the line profile to a Lorentzian shape.[54,55] Saturation broadening needs to be accounted for deducing the velocity distribution function. While fully saturated LIF has been used to get a better signal-to-noise ratio, it is difficult to determine the fully saturated regime and maintain such saturation over the entire interrogation volume.[52,53] For TALIF measurements, the used laser energy is in the quadratic regime where the TALIF intensity is proportional to the square of the laser energy to avoid the consequences of saturation effects described above. LIF signal intensities can be reduced due to quenching of the excited state by the feed gases, humidity, air, and molecular gases such as the ones used in the microelectronics industry. A correction of the fluorescence intensity due to the presence of such quenchers needs to be accounted to obtain absolute densities.[56–58] Resonant transitions from the ground state are often not available for all atomic and molecular species. Excitation from the metastable states of neutrals and ions has been used as a proxy for ground state species by assuming thermal equilibrium between the metastable and the ground states. This allows to obtain useful information about species velocities that are important for applications with plasma flows such as ion sources and plasma thrusters.[55,59–61] The metastables in a plasma are predominantly produced by the presence of

electrons with the appropriate energy. The absence of electrons with such energy, quenching due to collisions, or ionization can deplete or reduce the density of the metastable states below the detection limit of LIF. Hence, the application of LIF for metastable excitation may not be applicable to a wide variety of discharge environments.

B. Implementation and instrumentation

The laser beam is focused on to the plasma and the fluorescence is typically detected perpendicular to the laser beam propagation by a detector [Fig. 1(b)]. The spatial resolution in LIF is limited by the focus size of the laser launch and the collection optics. The fluorescence from the region probed by the laser beam is imaged onto the detector by using a lens. Using a PMT results in a point measurement and the spatial distribution can be obtained by using diaphragms and positioning the PMT to image different regions of the laser beam. The wavelength of fluorescence is typically different from the laser excitation wavelength. However, fluorescence detection at the same wavelength as the excitation wavelength has also been reported.[45] In such situations, fluorescence is detected with a certain delay after the laser beam. This technique relies on the longer lifetime of the laser excited level than the pulse width of the laser beam. When the laser excitation wavelength is different from the fluorescence wavelength, an appropriate narrow band-pass filter or a cut-off filter is installed in front of the detector to transmit only the fluorescence onto the detector or block the Rayleigh scattering of the laser beam. When a fluorescence spectrum is desired, the laser beam is imaged onto the entrance slit of a monochromator that is coupled with an iCCD camera or a PMT. The shaping of the laser beam into a sheet provides a two-dimensional distribution of the imaging species and this technique is called planar laser-induced fluorescence (PLIF).[62–65] PLIF can provide the spatial distribution of nonuniformities in the discharge with a single measurement [Fig. 1(b)]. Examples of the measured OH density using LIF and PLIF are
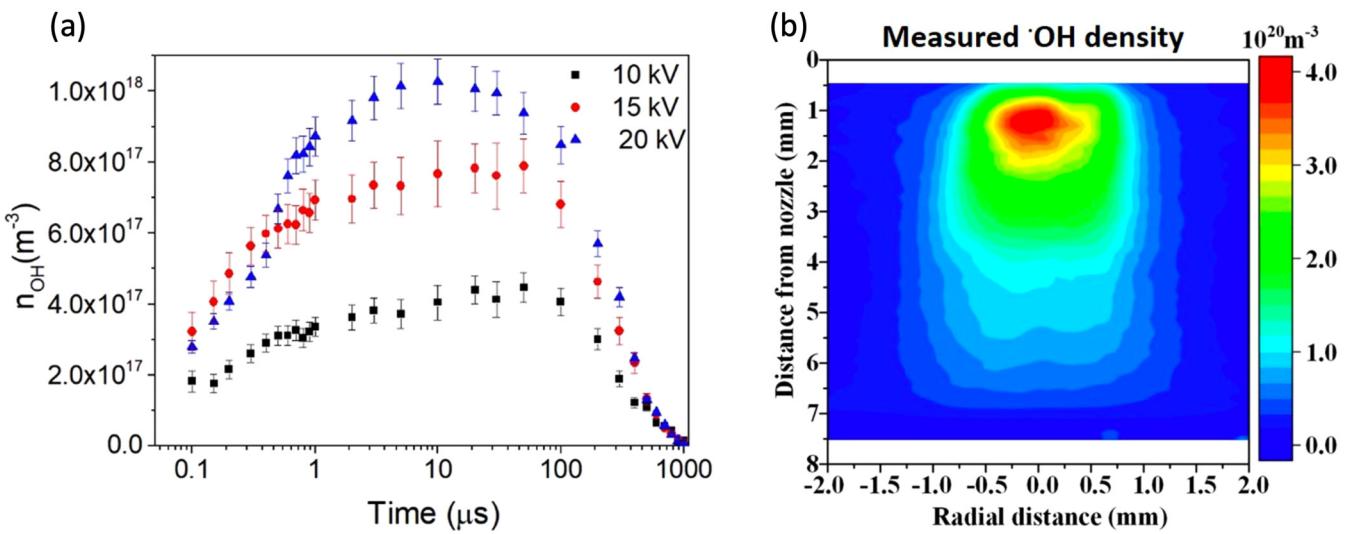
FIG. 2. Examples of absolute OH density measured using (a) LIF of a pulsed dielectric barrier discharge [Reprinted with permission from Yatom and Dobrynin, J. Phys. D: Appl. Phys. **55** (2022). Copyright 2022, IOP Publishing] and (b) PLIF of an RF plasma jet [Reprinted with permission from Kondeti *et al.*, J. Vac. Sci. Technol. A **38** (2020). Copyright 2020, American Vacuum Society].

shown in Figs. 2(a) and 2(b). For obtaining time-resolved information on the plasma-produced species in a pulsed plasma, a pulsed laser is typically used. The temporal resolution is limited by the pulse width of the laser beam. An example of the time-resolved OH density measured in a pulsed plasma is shown in Fig. 2(a). Nanosecond pulsed laser beams are a popular and a cost-effective way for executing LIF, while the relatively more expensive picosecond and femtosecond lasers have also been used for performing LIF.[66–68] One-dimensional and two-dimensional distributions of species have been reported using LIF/PLIF.

Depending on the application, different types of lasers have been used to perform the LIF measurements. These include solid state lasers, dye lasers, diode lasers, quantum cascade lasers, and optical parametric oscillators (OPOs).[70,71] Diode lasers can have a linewidth down to the fm range, while dye lasers typically have linewidths in the pm range, and commercial OPO lasers have linewidths in the range of tens to hundreds of pm. The narrow linewidth of diode lasers allows the accurate resolution of the narrow spectral features of atomic, ionic, and molecular transitions. These lasers can be applied to detect precise Doppler shifts in the transition. These shifts can be caused by velocity changes as small as tens of m/s along the direction of the laser beam propagation (Sec. II F). The inherent large linewidths of the dye lasers and the OPO lasers compared to the diode lasers limit their application to measuring only large Doppler shifts that are produced by very high ion or atom velocities.[72] The dye lasers and the OPO lasers offer the ability to generate a broad range of wavelengths ranging from the deep ultraviolet (DUV) to the infrared region. Solid state lasers, diode lasers, and quantum cascade lasers often generate radiation only in a narrow spectral region and do not have the versatility to generate a broad range of wavelengths.

C. Calibration method for obtaining absolute density for LIF

The LIF signal can be calibrated to obtain absolute densities of the ground state species. The LIF signal can be described by the following equation:[51,73]

$$I_{LIF} = \frac{1}{4\pi} \int \left(\eta_{LIF} \frac{hc}{\lambda_{fl}} \right) n_{exc}(x, y, z, t) A_{fl} \, dx \, dy \, dz \, dt, \quad (1)$$

where η_{LIF} is the instrumental factor that is the product of quantum efficiency of the detector, transmission of the optical setup, and the solid angle of signal collection, h is the Planck's constant, c is the speed of light, $n_{exc}(x,y,z,t)(m^{-3})$ is the density of the excited level, from which the fluorescent photons are emitted, λ_{fl} is the fluorescence wavelength (m), and A_{fl} is the Einstein coefficient of the detected fluorescence transition (s^{-1}). The unknown parameters in this equation are η_{LIF} and n_{exc}. This section describes a method to calculate the ground state density n by using Rayleigh scattering and a population kinetics model.

1. Rayleigh scattering

The experimental setup for implementing this calibration method is similar to the experimental setup used for executing LIF [Fig. 1(b)]. The plasma is turned off and the region of interest is filled with a gas such as air. The spectral filter that was used for LIF is removed and the laser beam is imaged on to the detector to collect the Rayleigh scattering signal from air. If a monochromator was used for LIF, the wavelength window of the monochromator is adjusted to detect the Rayleigh scattering laser beam. The position of the detector is not changed compared to the LIF setup to ensure

that the solid angle of detection is the same as that for the LIF measurements.

The Rayleigh scattering signal (I_R) can be described as[51,73–75]

$$I_R = \eta_R N_n \left(\frac{\partial \sigma_0}{\partial \Omega} \right) E_L \Delta x, \tag{2}$$

where N_n is the scattering particles' density, E_L is the laser pulse energy, Δx is the detection volume length, η_R is the instrumental factor for the wavelength of the Rayleigh scattering, and $\frac{\partial \sigma_0}{\partial \Omega}$ is the Rayleigh scattering differential cross section. The differential Rayleigh scattering cross section depends on the polarization direction of the laser beam and the angle at which the scattering light is collected. A convenient configuration is when the polarization of the laser beam is perpendicular to the laser propagation direction and the Rayleigh scattering collection is at an angle of 90° with respect to the laser propagation direction and the polarization direction. Assuming that the detector collects all polarizations of the scattered beam, the differential Rayleigh scattering cross section is defined as[74]

$$\frac{\partial \sigma_0}{\partial \Omega} = \frac{3\sigma}{8\pi} \frac{2}{(2 + \rho_0)}, \tag{3}$$

where σ is the total Rayleigh scattering cross section (m^2) and ρ_0 is the ratio of the horizontal-to-vertical polarized light in an unpolarized laser beam. The subscript 0 corresponds to the detection of both horizontal and vertical polarization of the scattering. The values of σ and ρ_0 for the commonly used scattering from air are tabulated as functions of wavelength in the review by Miles *et al.*[74] Calibration using Rayleigh scattering is usually performed at a known pressure and temperature. The scattering particles' density can be obtained by using the ideal gas law,[76]

$$N_n = \frac{P}{k_B T}, \tag{4}$$

where k_B is the Boltzmann constant. To calculate the instrumental factor, η_R in Eq. (2), the Rayleigh scattering intensity is measured for several laser energies at a fixed pressure. The slope of the straight line curve (α) is calculated by plotting the Rayleigh scattering intensity (I_R) as a function of the product of the laser pulse energy, E_L and the pressure, P (Fig. 3),

$$\alpha = \frac{I_R}{PE_L} = \frac{\eta_R \Delta x}{k_B T} \left(\frac{\partial \sigma_0}{\partial \Omega} \right). \tag{5}$$

The instrumental factor reduces to

$$\eta_R = \frac{\alpha k_B T}{\left(\frac{\partial \sigma_0}{\partial \Omega} \right) \Delta x}. \tag{6}$$

The wavelength of the LIF signal is different from the laser excitation wavelength. The instrumental factor depends on the efficiency of the detector at the wavelength of detection. Hence, the instrumental factor for LIF needs to be corrected for the detector efficiency at the two different wavelengths. So, $\eta_{LIF} = \eta_R \frac{\epsilon_{LIF}}{\epsilon_R}$, where
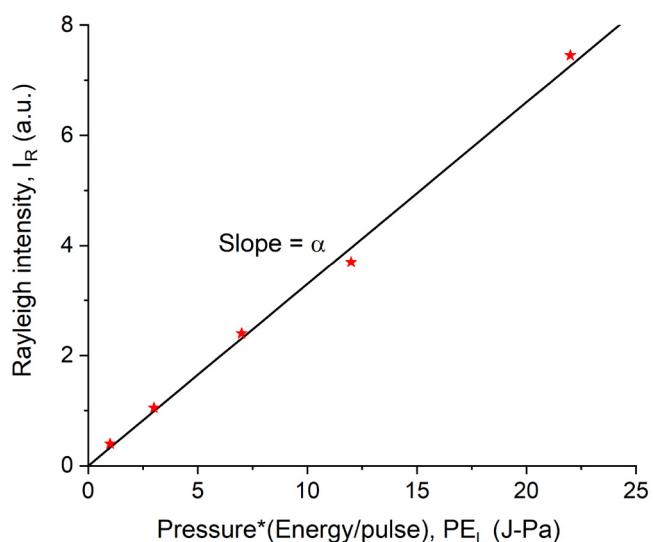
FIG. 3. Example to determine the instrumental factor by Rayleigh scattering. Experimental data have been adapted with permission from Yatom *et al.*, Plasma Sources Sci. Technol. **32** (2023). Copyright 2023, IOP Publishing.

ϵ_{LIF} and ϵ_R are the products of the transmission factor of optics and the quantum efficiency of the detector at the LIF and Rayleigh scattering wavelengths, respectively. This correction can be avoided by setting the laser wavelength to the LIF wavelength for Rayleigh scattering measurements. However, a large difference between the LIF wavelength and the laser excitation wavelength for such a measurement might shift the laser beam path, the energy density of the focused laser beam can be different, and such a large wavelength shift may not be in the tunable range of the laser being used.

2. Laser parameters and population kinetics model

Several parameters are required to be developed for the population kinetics model and we define them here. The time evolution of the laser irradiance [$I_L(t)$] is defined as[51,73]

$$I_L(t) = \frac{E_L \Gamma^{\langle 1 \rangle}}{\Delta \nu_L \tau_L A_L} L(t), \tag{7}$$

where $\Gamma^{\langle 1 \rangle}$ is the dimensionless one-photon overlap integral, $\Delta \nu_L$ is the laser linewidth (m^{-1}), A_L is the area of the laser beam at the detection location (m^2), and $L(t)$ is a normalized function that describes the temporal evolution of the laser pulse. $\Delta \nu_L$ can be obtained from the specifications sheet of the laser. A_L can be measured by a laser camera. Assuming the beam profile of the laser beam, it can also be calculated by measuring the residual laser energy by traversing a knife edge at the measurement location. I_L can be measured by measuring the Rayleigh scattering intensity with a short gate time at different delay times with respect to the laser beam. The dimensionless one-photon overlap integral is defined as[77]

$$\Gamma^{<1>} = \Delta v_L \int_{-\infty}^{+\infty} P_{abs}(v) P_L(v)\, dv, \qquad (8)$$

where P_{abs} is the absorption transition spectral profile (m) and $P_L(v)$ is the laser spectral profile (m). P_{abs} can be calculated by measuring the absorption profile and accounting for the different broadenings such as Van der Waals broadening and Doppler broadening.[51,69,73] If available, $P_L(v)$ can be taken from documentation of the laser manufacturer. The laser linewidth can be measured using methods such as heterodyne and etalon based techniques.[78,79]

The LIF signal is related to the population density of the excited state state species n_{exc} [Eq. (1)]. A population kinetics model is used to deduce the ground state density. We illustrate a three-level model here (Fig. 4); 4-, 5-, and 6-level models have also been implemented[41,51,73,80,81] together with models considering the full vibrational-rotational levels.[82,83] Upon laser irradiation, several processes occur that result in the measured LIF signal. These include laser excitation from the ground state to the excited state, laser de-excitation from the excited state to the ground state, spontaneous relaxation from the excited state to any lower energy level, and collisional quenching of the excited state. While there can be an additional source of production that can increase the density of these different levels, it is usually accounted for by removing their contribution by taking a background signal. The background signal is measured by de-tuning the laser from the LIF transition or by turning off the laser beam. The model assumes the level being measured to be in a quasi-steady state, where the laser excitation and its subsequent de-excitation is the most dominant process that results in the changes of the population of these states. A set of time dependent differential equations are solved to obtain the ground state density.[41,51,73,80,81]

The time dependent differential equations for a three-level model are described below,

$$\frac{dN_1}{dt} = I_L(t)\left(B_{21} N_2 f_B^2 - B_{12} N_1 f_B^1\right) + A_{21} N_2, \qquad (9)$$
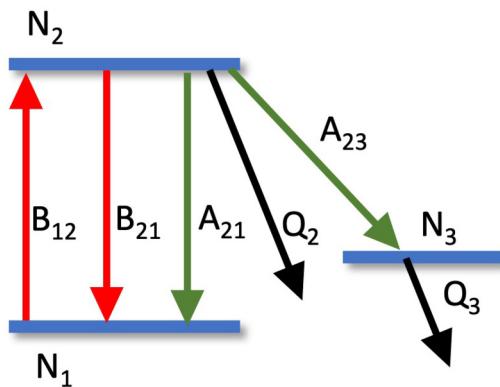

FIG. 4. Three-level model of LIF. A_{ij}, spontaneous optical transitions, B_{ij}, laser-induced transitions, Q, collision induced transitions.

$$\frac{dN_2}{dt} = I_L(t)\left(B_{12} N_1 f_B^1 - B_{21} N_2 f_B^2\right) - Q_2 N_2, \qquad (10)$$

$$\frac{dN_3}{dt} = A_{23} N_3 - Q_3 N_3, \qquad (11)$$

where N_i is the density of level i normalized to the ground state species density n, $I_L(t)$ is as defined in Eq. (7), B_{ij} is the Einstein B coefficient from level i to level j (mJ^{-1}), A_{ij} is the Einstein A coefficient from level i to level j (m^3 s^{-1}), f_B^i is the temperature-dependent Boltzmann factor of level i, i.e., the fraction of molecules in level i, and Q_i is the quenching rate of level i. The Einstein A coefficient, the Einstein B coefficient, and the Boltzmann factor are available from literature for several species.[84] This information is not readily available for all species of interest. The Einstein A coefficient for atomic species is available from the NIST database,[84] while it is available for several molecular species in the cited references in the tables.[85] The Einstein B coefficients are available for well studied species in the references provided in the tables. The Boltzmann factor needs to be calculated for the specific energy levels involved in the transitions.[86,87] For the ground state and the metastable level atomic species, the Boltzmann factor can be assumed to be unity. However, for resonant atomic levels, the population of the resonant levels need not be larger than the other resonant levels involved in the transitions. For example, LIF can be performed by exciting the Ar(1s$_2$) and the Ar(1s$_4$) resonant levels, which are the ground states for the excitation of these species. The validity of f_B being taken as unity needs to carefully examined for each case. Q_2 can be estimated by measuring the fluorescence decay time constant after accounting for the collisions with different species.[51] These equations are solved to obtain the ground state density of the species.

A two-level population kinetics model is a simplification of the three-level population kinetics model. An analytical solution exists for a two-level model under steady state conditions. In a two-level model, the level N_3 is ignored and the rate Eqs. (9) and (10) are solved. Equation (1) reduces to the following:

$$I_{LIF} = N_{total} B_{12} I_L \frac{A_{21}}{A_{21} + Q_2 + (B_{21} + B_{12}) I_L} \frac{\Omega}{4\pi}, \qquad (12)$$

where N_{total} is the the sum of N_1 and N_2. When LIF is performed with a low laser energy that follows the linear LIF regime, $(B_{21} + B_{12}) I_L \ll A_{21} + Q_2$, Eq. (12) reduces to the following:

$$I_{LIF} = N_{total} B_{12} I_L \frac{A_{21}}{A_{21} + Q_2} \frac{\Omega}{4\pi}. \qquad (13)$$

The factor $\frac{A_{21}}{A_{21}+Q_2}$ is often referred to as the fluorescence efficiency, similar to the often used branching ratio in TALIF calculations [Eq. (16), see further]. This factor is small at high pressures due to the increase in the contribution of quenching (Q_2). For quantitative measurements, it is important to have an estimate of quenching. When the used laser energy is sufficiently high to be under the saturated regime $((B_{21} + B_{12}) I_L \gg A_{21} + Q_2)$, Eq. (12)

reduces to the following:

$$I_{LIF} = N_{total} B_{12} I_L \frac{A_{21}}{(B_{21} + B_{12})I_L} \frac{\Omega}{4\pi}. \tag{14}$$

Working in the saturation limit eliminates the LIF signal dependence on laser energy and quenching. It simplifies the deduction of the densities. However, reaching the saturation limit depends on quenching and it is often not straightforward to know whether the saturation limit is reached. The steady state two-level model is the simplest form of the population kinetics model and provides an order of magnitude estimate of the density. Models that consider more levels have been implemented for more accurate estimates.

Verreycken et al.[75] compared a six-level population kinetics model to a four-level population kinetics model. Both the models gave similar densities of OH radicals in an atmospheric pressure plasma jet. The assumption of infinitely fast rotational energy transfer compared to quenching, emission, and vibrational energy transfer in the four-level population kinetics model did not result in a significant difference in the calculated density compared to the 6-level population kinetics model. They evaluated the effect of inaccuracy in different parameters used in the calculation and reported the main source of inaccuracy in the LIF calibration by Rayleigh scattering that comes from the laser linewidth.

D. Other calibration methods

The LIF intensities can be calibrated using a known concentration of the species being measured. Reference LIF signals from stable gases such as NO have been used as a reference to calibrate the fluorescence intensities to obtain absolute densities.[88] Other methods such as absorption spectroscopy have been used to obtain the absolute densities and validate densities calculated by the population kinetics models.[75]

E. Calibration using a known concentration of a gas for TALIF

TALIF is a nonlinear two-photon excitation process.[66] This does not allow the use of Rayleigh scattering to calibrate the fluorescence intensity to deduce the absolute density of the species discussed in Sec. II C 1. The experimental setup for TALIF calibration is the same as the setup used for collecting the TALIF signal [Fig. 1(b)]. In this method, a known concentration of a reference gas is excited to a higher level using two-photon excitation by a laser. The reference gas is chosen such that the two-photon excitation wavelength of the reference gas is spectrally similar to the excitation wavelength of the species whose absolute density needs to be determined. The position of the detector for the TALIF of the measured species and the reference gas setup is the same. The TALIF signal from the reference gas can be collected by using an appropriate spectral filter or by setting a monochromator to transmit the desired wavelength. The used laser energy is in the quadratic regime for both the reference gas and the detection species to avoid correction for the complicated saturation effects. The TALIF signal

(I_{TALIF}) can be defined as[56,57,66]

$$I_{TALIF} = T \frac{\sigma^{(2)} a \Gamma^{\langle 2 \rangle} n}{(h\nu)^2}, \tag{15}$$

where T is the instrumental factor, $\sigma^{(2)}$ is the two-photon absorption cross section, $h\nu$ is the photon energy, $\Gamma^{\langle 2 \rangle}$ is the dimensionless two-photon overlap integral between the laser spectral profile and the two-photon absorption profile[77], and n is the species density. $\sigma^{(2)}$ is available for different species in the cited references of the tables. The branching ratio (a) is defined as[57,66]

$$a_i = \frac{A_{ik}}{A_i + \sum_q k_q n_q}, \tag{16}$$

where the subscript q refers to the quenching species, A_{ik} is the spontaneous emission coefficient of the observed fluorescence line from level i to level k, A_i is the total spontaneous emission rate from the excited level i, k_q is the quenching coefficient, and n_q is the density of the quenching species assuming that the three-body collisional quenching is negligible.[89]

The dimensionless two-photon overlap integral is the two-photon analog to the one-photon overlap integral defined in Eq. (8). It is defined as[77]

$$\Gamma^{\langle 2 \rangle} = \Delta \nu_L \int_{-\infty}^{+\infty} \int_{-\infty}^{+\infty} P_{abs}(2\nu) P_L(\nu) P_L(\nu)\, d\nu\, d\nu. \tag{17}$$

TALIF signals from both the reference gas (I_r) and main species (I_m) are collected. The density of the main species reduces to[66]

$$n_m = \frac{T_r}{T_m} \frac{\sigma_r^{(2)}}{\sigma_m^{(2)}} \frac{a_r}{a_m} \left(\frac{h\nu_m}{h\nu_r}\right)^2 \frac{I_m}{I_r} \frac{\Gamma_r^{\langle 2 \rangle}}{\Gamma_m^{\langle 2 \rangle}} n_r, \tag{18}$$

where the subscripts m and r refer to the main species and the reference gas, respectively.[66,89]

F. Laser-induced fluorescence for velocity distribution functions

LIF is a crucial optical measurement technique for characterizing the flows and studying the kinetic processes in plasmas.[55,90,91] LIF allows for the measurements of the VDF, which is essential for understanding the thermodynamic state of a medium. This function allows us to derive important parameters such as the temperature, mean velocity, and the most probable velocity from the fluorescence profile. Moreover, LIF can directly measure the electric and magnetic fields in plasmas through the Stark[92] and the Zeeman effect[93], respectively. It is also possible to indirectly determine the electric fields by analyzing the moments of the VDFs.[94] LIF utilizes the Doppler effect, where the absorption of light occurs at a frequency shifted from the resonant transition frequency, a shift that depends on the velocity of the moving atom or the ion. Thus, it is sometimes referred to as the Doppler-shift LIF.
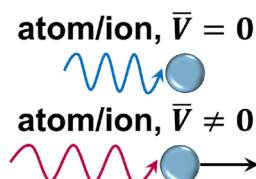
FIG. 5. Schematic of the Doppler effect.

The LIF process consists of two steps, as illustrated in Fig. 1(a). In the first step, the species in the plasma are often in the excited state due to collisions with energetic electrons or other species. These states, known as the metastable states, have long lifetimes—up to seconds, compared to the fluorescence states. It is important to note that when a metastable state is excited to deduce the properties of the ground state species, an assumption about the thermal equilibrium between this state and the ground or other states of the probed species in the plasma is necessary. When a laser beam is introduced, these excited atoms or ions absorb photons and are further excited to a higher energy state. The selection of this transition is guided by rules based on various quantum numbers[95] and must be sufficiently populated to ensure a detectable signal.[96] Plasma parameters, such as the electron temperature and the electron density, influence the excitation rate and de-excitation mechanisms such as quenching (e.g., collisions). To

facilitate further excitation to a higher state, photon energy (wavelength) of the laser must correspond precisely with the energy required for a resonant transition. However, due to thermal or directional motion of the probed species in the plasma, they perceive the incoming laser light wavelength Doppler-shifted (see Fig. 5). This requires tuning of the laser wavelength to the target species moving at specific velocities.

In the second step of the process, the excited species emit light through spontaneous emission, collisions, or stimulated emission, transitioning to a lower energy state. This transition can be resonant, in case if the species return to their initial energy state, and nonresonant if decay leads to a different level. Non-resonant emission is typically utilized in Doppler-shift LIF diagnostics because it allows the emitted wavelength to be easily distinguished from the intense laser light. The intensity of the emitted light is directly proportional to the number of species moving at the targeted velocity. By measuring emissions at various excitation frequencies, one can reconstruct the VDF, yielding detailed parameters of the ions or the neutrals. A schematic of this process is shown in Fig. 6(a). When the laser frequency is scanned across the Doppler broadened absorption profile, the excited species then emit the fluorescence light. This signal is detected by various methods described in Sec. II F 3, and the profile of the VDF can be reconstructed [Fig. 6(b)]. The doppler-shift LIF can be characterized with a high spatial resolution of 100's of μm,[97] a temporal resolution of 10's of μs,[98–100] and a spectral resolution, which in terms of velocity translates to as low as a few m/s.[101]
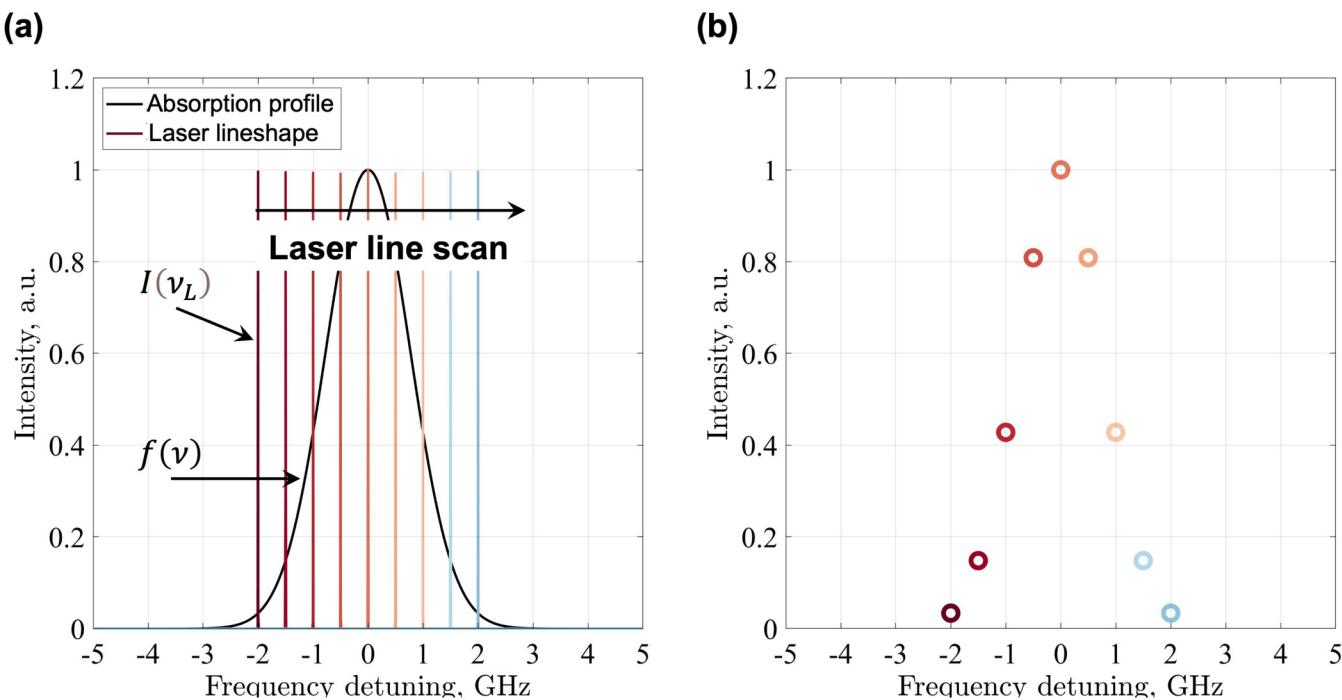

FIG. 6. Schematic of the LIF measurements. (a) Laser wavelength ($I(\nu_L)$) is scanned across the Doppler broadened absorption profile ($f(\nu)$). (b) The recovered signal, which is proportional to the integral: $\int f(\nu) I(\nu_L) d\nu$. ν_L: laser wavelength.

1. Line shape

While Doppler broadening is the primary effect that allows us to extract information about the shape of the VDF, it is crucial to consider other mechanisms that might affect the measured line shape profile. In this subsection, we will discuss several physical mechanisms that contribute to the broadening of the line shape. Typically, the profile is influenced by broadening mechanisms such as hyperfine structure, isotopic splitting, Zeeman splitting, lifetime broadening, or Stark broadening. It is crucial to note that the VDF measurements are feasible only under conditions where pressure broadening is not significant compared to the measured linewidth of the LIF transition. This depends on the transition being probed and the operating conditions, for example at a pressure < 10 Torr.[102] The measured LIF profile, denoted as $f_{LIF}(\nu_L)$, results from the convolution of the Doppler line shape with the effects of broadening mechanisms and the laser intensity. This relationship can be represented mathematically as follows:

$$f_{LIF}(\nu_L) \propto f(\nu_L) \otimes \phi_L(\nu_L) \otimes \phi_b(\nu_L), \quad (19)$$

where $f(\nu_L)$ represents the amplitude of the Doppler line shape, $\phi_L(\nu_L)$ is the laser intensity profile (typically negligible), and $\phi_b(\nu_L)$ includes all broadening mechanisms, and is referred to as the Doppler-free line shape.

Doppler broadening arises from the thermal and directional velocities of the species being probed. Consider a laser with a frequency of ν_L and a wave-vector of $\mathbf{k}$. For a moving particle with velocity $\mathbf{v}$, the shift in the laser frequency, $\Delta\nu$ in the species frame is given by

$$\frac{\Delta\nu}{\nu_L} = -\frac{\mathbf{v}\cdot\mathbf{k}}{c}, \quad (20)$$

where c is the speed of light. The transition frequency ν_T, at which the particle absorbs the laser, then becomes

$$\nu_T = \nu_L + \Delta\omega = \omega_L\left(1 - \frac{\nu_k}{c}\right), \quad (21)$$

where (ν_k) is the velocity component along $\mathbf{k}$. This establishes a direct correlation between the laser frequency and the particle velocities, facilitating the measurement of the VDF. LIF diagnostics involve scanning laser frequencies near the target transition and recording the fluorescence. Each frequency corresponds to a velocity group (ν_k) of the species, allowing the velocity distribution to be mapped as a function of the laser frequency,

$$f_{LIF}(\nu_k) \sim F\left(\frac{\nu_T}{1 - \nu_k c}\right). \quad (22)$$

This approach provides a one-dimensional representation of the VDF along the laser beam direction.

The broadening of the line shape due to the hyperfine structure of the energy levels and isotope splitting significantly impacts the spectral profile. The hyperfine energy levels are determined by the total angular momentum $\mathbf{F}$, which results from the coupling between the total electron angular momentum $\mathbf{J}$ and the nuclear

spin $\mathbf{I}$, represented as $\mathbf{F} = \mathbf{J} + \mathbf{I}$. For example, among the nine isotopes of xenon, seven have zero nuclear spin due to an even number of neutrons, and thus, do not contribute to hyperfine structures, leaving only two isotopes that affect the line shape. This complexity in the hyperfine structure[103] can complicate spectral analysis, especially since not all transitions have well-documented hyperfine structures. However, the most probable velocities can be discerned from the location of the LIF signal peak, which remains unaffected by this broadening mechanism. This allows for the characterization of flows and their variations. However, for a more comprehensive analysis, it is important to know the hyperfine structure and isotope splitting of the species.

The lifetime broadening mechanism is related to the Heisenberg uncertainty principle, which posits that certain pairs of physical properties, like position and momentum or energy (E) and time (t), cannot be precisely measured simultaneously. This principle is mathematically expressed as

$$\Delta E \Delta t \geq \hbar. \quad (23)$$

The uncertainty in the photon energy, $\Delta\omega$, is influenced by the lifetime of the upper energy level, τ_p. This relationship modifies the line shape into a Lorentzian function, as outlined in the literature,[104]

$$\phi(\nu) = \frac{\Delta\nu}{(\nu - \nu_0)^2 + (\Delta\nu/2)^2}, \quad \Delta\nu = \frac{1}{\tau_p}. \quad (24)$$

For instance, for the metastable level $5d^2[4]_{7/2}$ of Xe II, the lifetime ranges from 7 to 9 ns. The resultant broadening is significantly smaller by one or two orders of magnitude than that caused by Doppler broadening, and thus, can generally be neglected in analysis.

Two other mechanisms responsible for spectral line splitting are the Stark and the Zeeman effects. The Stark effect involves line splitting due to the strong electric fields, which can induce additional angular momentum between the nucleus and the electron cloud. However, the electric fields must be considerably strong to have a measurable impact. For instance, it was demonstrated that the Stark effect is negligible under typical plasma experimental conditions due to the field strengths involved.[105] On the other hand, the Zeeman effect, which results from the influence of the magnetic fields, is more significant and can substantially alter the LIF line shape.[102] This effect allows for the simulation of the spectral line splitting and the deduction of local magnetic field values, providing valuable insights into the magnetic environment within the plasma.

2. Laser systems

A tunable laser is essential for scanning the absorption profile in LIF experiments. It is important to distinguish between the continuous and the pulsed modes of the laser operation.[70,71] Continuous wave (CW) lasers, such as laser diodes, have extremely narrow bandwidths, typically in the femtometer range or below. They allow for the direct observation of the species' VDF in the LIF measurements. Pulsed lasers, in contrast, are broader in their linewidth and deliver a large amount of energy per pulse, with pulse

widths as short as a few femtoseconds, making them more suitable for time-resolved measurements.

The measurable VDFs vary with the type of the laser: diode lasers measure in the range of tens of m/s, while dye lasers and OPOs can detect velocities up to a few km/s and tens of km/s, respectively. As an example, the dependence of the laser linewidth ($\Delta\lambda$) in pm on the ion velocity for argon and xenon ions has been shown in Fig. 7. Diode lasers are particularly effective for measuring the profiles of the velocity distributions, whereas dye and OPO lasers are better suited for detecting velocity drifts in systems with high-energy flows. However, it is important to note that in the case of high-resolution measurements, the limiting factor is usually a resolution of the measurement system that detects the current laser wavelength, e.g., a wavemeter.

CW diode lasers are commonly used in Doppler-shift based LIF, especially for noble gases. They offer wide tunability (up to 10 nm, depending on the design) and very narrow linewidth. Additionally, they facilitate various high-frequency laser light modulations, such as amplitude and wavelength (or frequency) modulations, which are crucial for implementing detection methods based on homodyne,[106] heterodyne,[49] or photon counting principles.[107,108]

3. Optical setup

The typical optical setup for the Doppler LIF measurements can be divided into two main components: the laser launch branch and the detection branch, as illustrated in Figs. 8(a) and 8(b). The
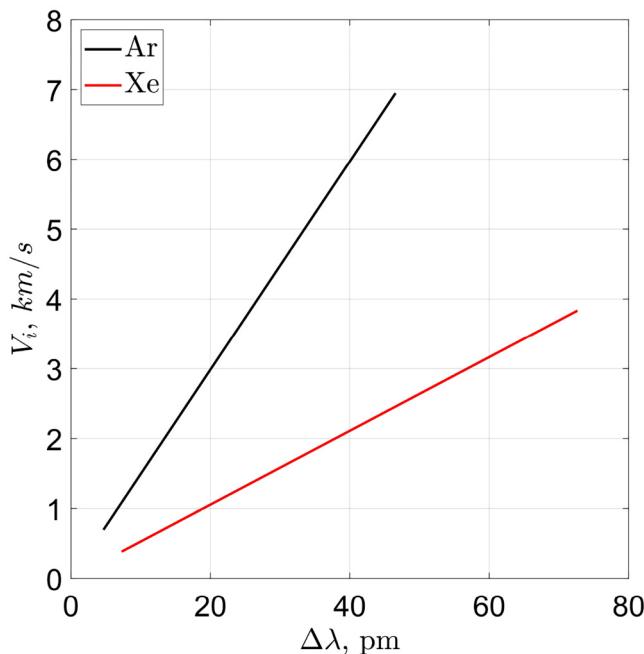

FIG. 7. Detectable argon and xenon ion velocities V_i as a function of the laser linewidth, $\Delta\lambda$. The wavelengths considered for the excitation of the Ar and Xe ions are 667 and 834 nm, respectively.

laser launch branch consists of optical elements tasked with beam conditioning, directing, light modulation, and the measurement of the laser power and the laser wavelength. The beam conditioning involves a series of mirrors and lenses that direct and focus the laser beam into the interrogation volume. Optical fibers may also be used to transport the laser beam. In some setups, the laser beam is shaped into a laser sheet for planar LIF measurements.[109] The laser wavelength is controlled using a calibrated wavemeter. Additionally, a Fabry–Pérot interferometer can be employed to monitor the quality of the laser mode in real-time and to detect any mode hops. The power of the beam is typically monitored continuously with a photodiode. The modulation of the laser wavelength or amplitude is an essential aspect of the setup. Amplitude modulation can be achieved using mechanical choppers, acousto-optic modulators (AOMs), or electro-optic modulators (EOMs). Wavelength modulation can be performed by modulating the laser diode current, which not only allows for high-frequency modulation but also results in amplitude modulation, or by using the piezo-driven modulation, which supports lower-frequency modulations without affecting the laser amplitude. Wavelength modulation is particularly useful for implementing the derivative spectroscopy techniques.[110,111]

The detection branch of the optical setup consists of a collecting lens that directs light through a series of lenses and a spatial filter (pinhole) into the detector. This lens is typically positioned so that its optical axis is perpendicular to the laser beam's wavevector, which enhances spatial resolution. The collected light is filtered around the fluorescence wavelength, either by a narrow bandpass filter or by a monochromator. Various detectors such as a photomultiplier tube (PMT), a photodiode, or a CCD camera can be used depending on the measurement requirements. For point measurements, a PMT is preferred due to its high sensitivity. A CCD camera is more suitable for planar LIF measurements. Additionally, the detection branch can be mounted on a movable stage, allowing measurements along the laser beam and enabling the acquisition of 1D distributions of parameters such as velocity and temperature.

Signal processing for the LIF measurements can be performed in various ways to achieve either time-averaged or time-resolved information. A lock-in amplifier, synchronized with the laser modulation frequency, is commonly used. For more advanced techniques, utilizing beating frequencies help in the extraction of time-resolved information effectively. The photon-counting technique is also widely employed for this purpose. When the laser wavelength is modulated, the use of a lock-in amplifier to extract higher harmonics facilitates the derivation of the VDF profile. This technique provides a more sensitive analysis of the true VDF shape, particularly in cases of complex signals that deviate from a Maxwellian distribution. When single-photon counting method is used, a multichannel scaler can also be used to count the signal pulses.[112] The signal measured during each laser pulse period can be accumulated to measure the fluorescence waveforms.

The placement of the detection branch perpendicular to the laser beam typically necessitates at least two optical ports in the plasma chamber: one for the entry of the laser and another for collecting the LIF signal. However, modern industrial-scale plasma reactors are fully enclosed to ensure uniform processing of the materials and having more than one viewport can disrupt the

(a)

(b)
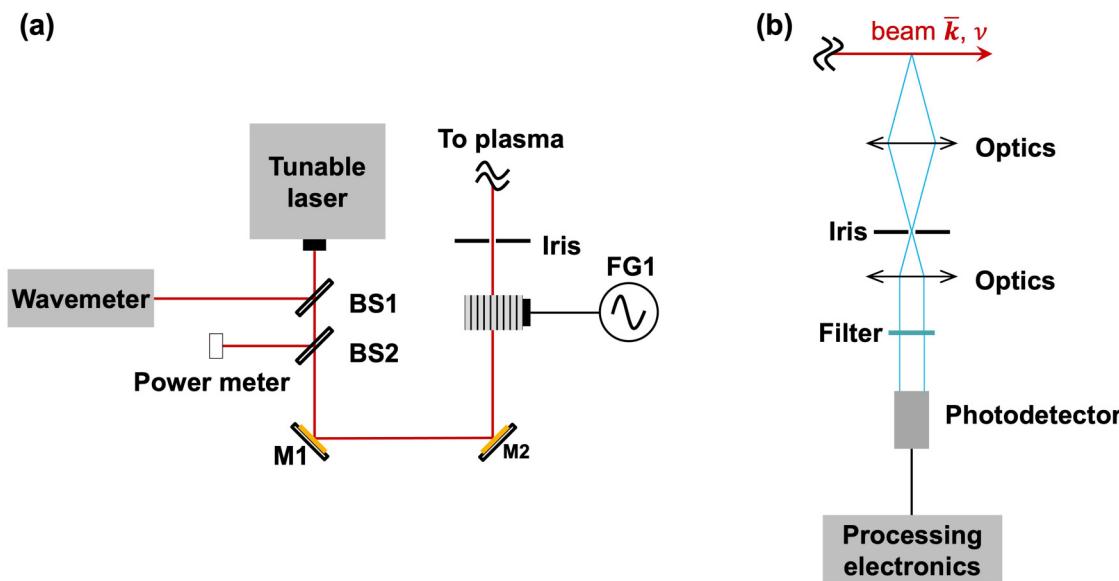
FIG. 8. Generalized LIF setup. (a) Laser launch brunch, BS1,2 are beam splitters, and M1,2 are mirrors. (b) Detection branch. "Optics" can represent various combinations of lenses arranged to collect fluorescent light.

plasma processes and alter the processing of the material. Additionally, space constraints often limit access to only one location around a plasma reactor. In such cases, confocal LIF is a suitable alternative. This technique allows both the input laser beam and the collected LIF signal to pass through the same axis into the plasma discharge, minimizing the need for multiple ports. Originally widespread in the fields of biology and medicine,[113] confocal LIF has been adapted for TALIF and single LIF measurements across various scenarios.[114–117] Recently, this method has been enhanced with structured laser light, specifically Laguerre–Gaussian beams, to improve the signal-to-noise ratio. This modification has been successfully implemented on a plasma source to measure the velocity of argon ions.[118]

III. LIF/TALIF REFERENCE DATA

The microelectronics industry and sustainability applications use a combination of a wide variety of precursor gases such as CH_4, CF_4, CH_2F_2, CHF_3, C_2F_4, C_3F_6, C_4F_6, C_4F_8, NF_3, HBr, Cl_2, COS, SF_6, H_2, O_2, H_2O, N_2, He, and Ar, among others to generate the plasma.[56,119–132] It results in the generation of a combination of a wide variety of ions, radicals, and metastable species that play different roles in the overall chemical process. The LIF/TALIF transitions to detect such species should be carefully selected such that there is no overlap in the excitation and fluorescence wavelengths of the species of interest with other species present in the detection volume. There are several species that have coincident excitation and fluorescence wavelengths. Depending on the species present in the interrogation volume, the excitation and fluorescence wavelengths should be carefully examined to determine if a spectral filter or a monochromator is

required for collecting fluorescence. While using a spectral filter for collecting fluorescence often provides a higher optical efficiency, the presence of overlapping fluorescence might necessitate the use of a monochromator to obtain the wavelength of the fluorescence and differentiate between the interfering species. For example, in an industrial scale silicon etching CCP discharge with argon and oxygen admixture, we found that both the excitation and the fluorescence wavelengths of O_2^+ ions and SiO radicals coincide with one another inhibiting the differentiation between the two species even with the use of a monochromator. This reference data is intended to assist in the selection of the LIF/TALIF transitions that do not overlap with other species present in the interrogation volume. Some groups of species with overlapping excitation and fluorescence wavelengths that may not be differentiable by the use of a 10 nm (FWHM) spectral filter are listed in Table I.

A complied list of the available LIF/TALIF transitions for atomic, molecular, ionic, and metastable species relevant to the microelectronics industry and sustainability applications are shown in Tables II–V. Several of these transitions were studied a few decades ago when the availability and the use of equipment such as an iCCD camera or a monochromator were unavailable. When the transition/fluorescence information was unavailable, a "not-reported" (NR) indication was mentioned in the tables. Certain neutral molecules cannot be detected by excitation from the ground state and require the presence of higher vibrational states for their detection. They have been marked in the tables. While we have put efforts into reporting all the relevant species that have been reported in the literature, it is possible that the reported tables inadvertently omitted the relevant species/transitions that have been previously reported.

TABLE I. Overlapping laser-induced fluorescence transitions. ††: Laser excitation is from a vibrationally/rotationally excited state of a neutral gas molecule.

Sl. No.	Species	Transition	Excitation (nm)	Fluorescence (nm)	Reference
1	NO	$A^2\Sigma^- - X^2\Pi$	226–227	248	88, 133, and 134
	$O_2^{\dagger\dagger}$	$B^3\Sigma_u^- - X^3\Sigma_g^-$	223–226	240–440	135
	O_2^+	$X^2\Pi_g - A^2\Pi_u$	225–227	245	136
	SiO	$A\ ^1\Sigma - X^1\Sigma$	220–237	214–350	48, 137, and 138
2	CH_3O	$A^2A_1 - X^2E$	270–330	300–400	139–143
	OH	$X - A$	280–286	304–314	73, 75, and 144
	Ti	$^3D_{1,2,3}, {}^1F_3, {}^3F_3, {}^3G_3 - {}^3F_{2,3,4}$	221–296	250–341	145
3	CH_3O	$A^2A_1 - X^2E$	270–330	300–400	139–143
	SiCl	$B^2\Sigma - X^2\Pi$	275, 295, 308	280, 320, 290–307	146 and 147
	SiF	$X - B$	288	308–315	148
	Ti	$^3D_{1,2,3}, {}^1F_3, {}^3F_3, {}^3G_3 - {}^3F_{2,3,4}$	221–296	250–341	145
	W	$5d^46s^2\ ^5D_0 - 5d^5\ ^4D6s_1^0$	287.9	302.5	149 and 150
4	CF_3O	$\tilde{A}^2A_1 - \tilde{X}^2E$	332–352	355–400	151 and 152
	CN_2	$^3\Pi_1 - {}^3\Sigma^-, \tilde{A}^3\Pi - \tilde{X}^3\Sigma^-$	327–336	330–440	153–155
	C_2H_3O	$\tilde{B}^2A'' - \tilde{X}^2A''$	330–350	340–420	156–158
	C_2H_5O	$\tilde{A} - \tilde{X}$	310–350	340–430	139, 140, and 159
	HC_2O	$X^2A' - {}^2A''$	310–360	350–460	160
	NH	$A^3\Pi - X^3\Sigma^-$	303–305, 329–336	330–345	62 and 161–163
	N_2O^+	$\tilde{A}^2\Sigma^+ - \tilde{X}^2\Pi_i$	337–356	312–345	164
	SH	$^2\Sigma^+ - {}^2\Pi_{3/2,1/2}$	323–330	320–362	165–167
5	CH_2O	$\tilde{A}^1A_2 - \tilde{X}^1A_1$	352–357	380–550	168 and 169
	CN	$B^2\Sigma - X^2\Sigma$	356.5, 381–388.5, 565–610	388.8, 389.5	63 and 170–172
6	C_2H_5S	$\tilde{A} - \tilde{X}$	390–450	420–580	173
	C_3H_7S	$\tilde{A} - \tilde{X}$	395–430	420–520	174
	SiN	$\tilde{B}\ ^2\Sigma - \tilde{X}\ ^2\Sigma$	396	414	175
7	C_2H_5S	$\tilde{A} - \tilde{X}$	390–450	420–580	173
	C_3H_7S	$\tilde{A} - \tilde{X}$	395–430	420–520	174
	N_2^+	$B^2\Sigma_u^+ - X^2\Sigma_g^+$	391	428	43
8	C_2H_5S	$\tilde{A} - \tilde{X}$	390–450	420–580	173
	C_3H_7S	$\tilde{A} - \tilde{X}$	395–430	420–520	174
	CS_2^+	$X^2\Pi_{3/2} - A^2\Pi_{3/2}$	427–476	460–550	176
	HC_2S_2	$\tilde{B}^2A - \tilde{X}^2A$	435–458	458–530	177
	HSiF	$\tilde{A}\ ^1A'' - \tilde{X}\ ^1A'$	430, 446.5	425–530	178 and 179
9	Br_2^+	$^2\Pi_{u} - X^2\Pi_g$	472.7	480–640	180
	CuSH	$\tilde{A}\ ^1A'' - \tilde{X}\ ^1A$	472–515	480–506	181
	Na_2	$B^1\Pi_u - X^1\Sigma_g^+$	465.7–514.5	470–540	182
10	NO_3	$\tilde{B}^2E' - \tilde{X}^2A_2'$	500–680	464–662	183 and 184
	RuO	$[18.1]4 - X^5\Delta_4$	529.5–531	463–503	185
11	BO_2	$A^2\Pi_u - X^2\Pi_g$	579–583	538–554, 571–587, 611–627, 630–646	186
	Br_2	$B^3\Pi_{0^+u} - X^1\Sigma_g^+$	548–595	618–621, 714–1110	187 and 188
12	CH_2	$\tilde{b}\ ^1B_1 - \tilde{a}\ ^1A_1$	589–595	635–651	189
	C_2O	$\tilde{A}^3\Pi_i - \tilde{X}^3\Sigma^-$	588–685	650–780	190
	HNO	$\tilde{A}^1A'' - \tilde{X}^1A''$	623–626, 641.6–643	685–780	191–193
	NH_2	$\tilde{A}^2A_1 - \tilde{X}^2B_1$	571–662.2	516–824	194–196
13	SiCCl	$\tilde{A}^2\Sigma^+ - \tilde{X}^2\Pi$	550–615	545–650	197
	SiCF	$\tilde{A}^2\Sigma^+ - \tilde{X}^2\Pi$	574–604	547–596	198
14	SiCCl	$\tilde{A}^2\Sigma^+ - \tilde{X}^2\Pi$	550–615	545–650	197
	TiC	$^1\Pi - X^3\Sigma^+$	606.9–608.3	538–603	199
15	CH_2	$\tilde{b}\ ^1B_1 - \tilde{a}\ ^1A_1$	589–595	635–651	189
	C_2O	$\tilde{A}^3\Pi_i - \tilde{X}^3\Sigma^-$	588–685	650–780	190
16	C_2O	$\tilde{A}^3\Pi_i - \tilde{X}^3\Sigma^-$	588–685	650–780	190
	HNO	$\tilde{A}^1A'' - \tilde{X}^1A''$	623–626, 641.6–643	685–780	191–193
17	C_2P	$^2\Delta_i - \tilde{X}^2\Pi_r$	596–633	556–627	200

TABLE I. (*Continued.*)

Sl. No.	Species	Transition	Excitation (nm)	Fluorescence (nm)	Reference
	C$_2$S	$\tilde{A}^3\Pi_i - \tilde{X}^3\Pi^-$	675–690, 604–614	553–614	201
	HBF	$\tilde{A}^2A''\,\Pi - \tilde{X}^2A'$	602–666	535–628	202
	SiCl$_3$O	$\tilde{A}^2A_1 - \tilde{X}^2E$	590–650	617–653	203
	SiC$_3$H	$\tilde{A}^2\Sigma^+ - \tilde{X}^2\Pi_i$	613–681	578–663	204

TABLE II. Laser-induced fluorescence transitions of neutral molecular species. NR: not reported, ‡: absolute density reported, ††: Laser excitation is from a vibrationally/rotationally excited state of a neutral gas molecule.

Sl. No.	Species	Transition	Excitation (nm)	Fluorescence (nm)	Reference
1	AlO	B$^2\Sigma^+$ – X$^2\Sigma^+$	464–470	507–519	205–207
2	AlS	A$^2\Sigma^+$ – X$^2\Sigma^+$	418–430	440	208
3	As$_2$	A$^1\Sigma_u^+$ – X$^1\Sigma_g^+$	240–241	275–305	209–211
		A$^1\Sigma_u^+$ – X$^1\Sigma_g^+$	248	289.3	210
4	BC	B$^4\Sigma^-$ – X$^4\Sigma^-$	557.4–559.2	596.9	212 and 213
		E$^4\Pi$ – X$^4\Sigma^-$	290.9–291.5	*NR*	213
5	BCl	A$^1\Pi$ – X$^1\Pi^+$	272	278	214
6	BH	A$^1\Pi$ – X$^1\Sigma^+$	396	429–434	215 and 216
7	BH$_2$	$\tilde{A}^2B_1(\Pi_u) - \tilde{X}^2A_1$	727.2–742.4	*NR*	217
8	BO	A$^2\Pi$ – X$^2\Sigma^+$	313.5–316.5, 422–428, 434.5	*NR*	218 and 219
9	BO$_2$	A$^2\Pi_u$ – X$^2\Pi_g$	434–434.3	*NR*	218
		NR	545.6, 547.1	574–586	220
		A$^2\Pi_u$ – X$^2\Pi_g$	579–583	538–554, 571–587, 611–627, 630–646	186
10	BS$_2$	$\tilde{A}^2\Pi_u - \tilde{X}^2\Pi_g$	530–760	424–486	221
11	Br$_2$	B$^3\Pi_{0^+u}$ – X$^1\Sigma_g^+$	548–595	618–621, 714–1110	187 and 188
12	c–C$_6$H$_7$	$\tilde{A}^2A_2 - \tilde{X}^2B_1$	549.5–549.9	*NR*	222
13	CBr$_2$	$\tilde{A}^1B_1 - \tilde{X}^1A_1$	561–575	588–672	223 and 224
14	CCl	A$^2\Delta$ – X$^2\Pi$	278	*NR*	225 and 226
15	CCl$_2$	A$^1B_1$ – X$^1A_1$	416–556	391–500, >580	227–232
16	CCl$_2$S	$\tilde{B} - \tilde{X}$	274–297	*NR*	233
17	CF‡	A$^2\Sigma^+$ – X$^2\Pi$	223.8	230.6	234 and 235
18	CF$_2^‡$	$\tilde{A} - \tilde{X}$	260–276	260–390	235–238
19	CF$_3$O	$\tilde{A}^2A_1 - \tilde{X}^2E$	332–352	355–400	151 and 152
20	CF$_3$S	$\tilde{A}^2A_1 - \tilde{X}^2E_{3/2}$	373.8–374, 377.7–377.8, 365.8–366	*NR*	151
21	CFBr	$\tilde{A}^1A'' - \tilde{X}''A''$	422.6–424.8	416–556	239 and 240
22	CFCl	$\tilde{A} - \tilde{X}$	363.3, 367.3, 372.7, 378.3, 384	330–395	227, 231, and 241
23	CH‡	A$^2\Delta$ – X$^2\Pi$	431	489	242
		A$^2\Delta$ – X$^2\Pi$	427.9–428.1, 435.4–435.8	485	87 and 243
		B$^2\Sigma^-$ – X$^2\Pi$	363.3–363.6, 387–388	385–415, 423–435, 443–460	243–245
24	CHF	$\tilde{A}^1A'' - \tilde{X}^1A'$	492–493, 514.5, 574–582	515–521, 550–570, 600–620, 650–670	246–252
25	CH$_2$	$\tilde{b}^1B_1 - \tilde{a}^1A_1$	589–595	635–651	189
26	CH$_2$O	$\tilde{A}^1A_2 - \tilde{X}^1A_1$	352–357	380–550	168 and 169
27	CH$_3$O	A$^2A_1$ – X^2E	270–330	300–400	139–143
		$\tilde{B} - \tilde{X}$	357–376	316–375	253
28	CH$_3$S	$\tilde{A}^2A_1 - \tilde{X}^2E$	364–378	370–500	254 and 255
29	CN	B$^2\Sigma$ – X$^2\Sigma$	356.5, 381–388.5, 565–610	388.8, 389.5	63 and 170–172
30	CN$_2$	$^3\Pi_1 - {}^3\Sigma^-, \tilde{A}^3\Pi - \tilde{X}^3\Sigma^-$	327–336	330–440	153–155

TABLE II. (Continued.)

Sl. No.	Species	Transition	Excitation (nm)	Fluorescence (nm)	Reference
31	CO‡	B$^1\Sigma^+$ – X$^1\Sigma^+$	2 × 230.1	484	256 and 257
32	CO$_2$	(00^00) – (10^001)	2005, 2700	4260–4270	258 and 259
33	CS	A$^1\Pi$ – X$^1\Sigma^+$	257.5–258.3	250–290	260–262
34	CS$_2$	V^{1}B$_2$ – $\tilde{X}^1\Sigma_g^+$	280–338	370, 380, 403.7	263–266
35	CuSH	$\tilde{A}^1$A$''$ – $\tilde{X}^1$A$'$	472–515	480–506	181
36	Cu$_2$	A$^1\Sigma_u^+$ – X$^1\Sigma_g^+$	490.27	495–499	65
		B$^1\Pi_u$ – X$^1\Sigma_g^+$	449.8	460.7	267
37	C$_2^{\ddagger}$	d$^3\Pi$ – a$^3\Pi$	516	563	86
		d – a	470	425–438	87 and 268
		A$^1\Pi_u$ – X$^1\Sigma_g^+$	690.9	790.8	269–271
		d$^3\Pi_g$ – a$^3\Pi_u$	516.5	559	269 and 272
38	C$_2$H$_2$	$\tilde{A}$ – $\tilde{X}$	225–235	250–360	273
39	C$_2$H$_3$O	$\tilde{B}^2$A$''$ – $\tilde{X}^2$A$''$	330–350	340–420	156–158
40	C$_2$H$_3$S	$\tilde{B}$ – $\tilde{X}^2$A$''$	458.2–458.5	464–531	274
41	C$_2$H$_5$O	$\tilde{A}$ – $\tilde{X}$	310–350	340–430	139, 140, and 159
42	C$_2$H$_5$S	$\tilde{A}$ – $\tilde{X}$	390–450	420–580	173
		$\tilde{B}^2$A$'$ – $\tilde{X}^2$A$''$	397–427	352–425	275
43	C$_2$N	$\tilde{A}^2\Delta$ – $\tilde{X}^2\Pi$	465.8, 470–471.5	466–580	276 and 277
44	C$_2$O	$\tilde{A}^3\Pi_i$ – $\tilde{X}^3\Sigma^-$	588–685	650–780	190
45	C$_2$P	$^2\Delta_i$ – $\tilde{X}^2\Pi_r$	596–633	556–627	200
46	C$_2$S	$\tilde{A}^3\Pi_i$ – $\tilde{X}^3\Pi^-$	675–690, 604–614	553–614	201
47	C$_3$ ‡	A$^1\Pi_u$ – X$^1\Sigma_g^+$	405.3	398–411	278
		A – X	425–430	405	87
48	C$_3$H$_7$S	$\tilde{A}$ – $\tilde{X}$	395–430	420–520	174
49	C$_3$N	$\tilde{B}^2\Pi_i$ – $\tilde{X}^2\Sigma^+$	343–350	284–336	279
50	C$_4$H	$\tilde{B}^2\Sigma^+$ – $\tilde{X}^2\Sigma^+$	400–416.7	> 420	280
51	FCO	$\tilde{A}^2\Pi$ – $\tilde{X}^2$A$'$	307–345	333–477	281
52	GaCl	A$^3\Pi_0^+$ – X$^1\Sigma^+$	332–346	364	210
53	HBF	$\tilde{A}^2$A$''$ Π – $\tilde{X}^2$A$'$	602–666	535–628	202
54	HBr	M$^1\Pi$ – X$^1\Sigma^+$	115.2–116.2	NR	282
55	HCBr	$\tilde{A}$ – $\tilde{X}2_0^7$	560–561.3	468–528	224
56	HCl	V$^1\Sigma^+$ – X$^1\Sigma^+$	115.7–115.9	NR	282
57	HCO	$^2\tilde{A}$ – $^2\tilde{A}$	613–618	638–664	283
58	HC$_2$O	X^{2}A$'$ – ^{2}A$''$	310–360	350–460	160
59	HC$_2$S$_2$	$\tilde{B}^2$A$''$ – $\tilde{X}^2$A$''$	435–458	458–530	177
60	HC$_4$S	$\tilde{A}^2\Pi_{3/2}$ – $\tilde{X}^2\Pi_{3/2}$	487–501	426–488	284 and 285
61	HC$_6$S	$^2\Pi_{3/2}$ – $^2\Pi_{3/2}$	572–590	NR	286
62	HNO	$\tilde{A}^1$A$''$ – $\tilde{X}^1$A$'$	623–626, 641.6–643	685–780	191–193
63	HSiBr	$\tilde{A}^1$A$''$ – $\tilde{X}^1$A$'$	458–503	NR	287
64	HSiCl	$\tilde{A}$ A$''$ – $\tilde{X}$ A$'$	444–485, 538–550	471, 483, 489, 503, 524	288–290
65	HSiF	$\tilde{A}^1$A$''$ – $\tilde{X}^1$A$'$	430, 446.5	425–530	178 and 179
66	HSiNC	$\tilde{A}^1$A$''$ – $\tilde{X}^1$A$'$	499.75–502	428.2, 444.3, 461.9, 480.6	291
67	HSiNCO	$\tilde{A}^1$A$''$ – $\tilde{X}^1$A$'$	490–492	379.6–477.51	292
68	HSO	$\tilde{A}$ – $\tilde{X}$	539–540, 585, 600–615, 625–645	> 665	191 and 293–295
69	HSnCl	$\tilde{A}^1$A$''$ – $\tilde{X}^1$A$'$	455–500	389–482	296
70	H$_2$	E, F $^1\Sigma_g^+$ – X$^1\Sigma_g^+$	2 × 193.3	750, 830	297
	H$_2^{\dagger\dagger}$	B$^1\Sigma_g^+$ – X$^1\Sigma_g^+$	106.2–106.7	NR	298–300
71	InCl	A$^3\Pi_0^+$ – X$^1\Sigma^+$, B$^3\Pi_1$ – X$^1\Sigma^+$	340–360	363.7	210
72	IO	A$^2\Pi_{3/2}$ – X$^2\Pi_{3/2}$	435–468	500–600	301 and 302

03 December 2024 20:43:44

TABLE II. (*Continued.*)

Sl. No.	Species	Transition	Excitation (nm)	Fluorescence (nm)	Reference
73	I_2	$B^3\Pi_{0u}^+ - X^1\Sigma_g^+$	501.7, 514.5	515–830	303–305
74	KH	$A^1\Sigma^+ - X^1\Sigma^+$	502.4–504	548.5–557.5	306
75	K_2	$B^1\Pi_u - X^1\Sigma_g^+$	632.8	633–650	307
		$C^1\Pi_u - X^1\Sigma_g^+$	420–435, 457.9	420–475, 550–580	308 and 309
76	NaK	$D^1\Pi - X^1\Sigma^+$	476–529	1052–2500	310
77	Na_2	$B^1\Pi_u - X^1\Sigma_g^+$	465.7–514.5	470–540	182
78	NCO	A – X	420–440	465	194
79	NC_3O	$^2\Sigma - ^2\Sigma$	365.7–365.9	329–365	311
		$^2\Pi - ^2\Pi$	365.6–365.8	329–365	311
80	NC_3S	$\tilde{A}^2\Pi_{3/2} - \tilde{X}^2\Pi_{3/2}$	463.9–464.1	408–455	312
81	NF	$b'\,\Sigma - X^3\Sigma^-$	530	528.9	313
82	NH	$A^3\Pi - X^3\Sigma^-$	303–305, 329–336	330–345	62 and 161–163
83	NH_2	$\tilde{A}^2A_1 - \tilde{X}^2B_1$	571–662.2	516–824	194–196
84	NH_3	$X - C'$	2×305	550–575, 720	314
85	N_3	$\tilde{A}\,^2\Sigma^+ - \tilde{X}\,^2\Pi_{3/2}$	271.9	271.1–272.8	315
86	NO ‡	$A^2\,\Sigma^- - X^2\,\Pi$	226–227	248	88, 133 and 134
		$D^2\,\Sigma^- - X^2\,\Pi$	193	196–226	316
	NO ††	$C^2\,\Sigma^- - X^2\,\Pi$	193	208	316
87	NO_2	$\tilde{X}^2A_1 - \tilde{A}^2B_2$	434.9, 430.6, 435.1	638–663	317
88	NO_3	$\tilde{B}^2E - \tilde{X}^2A_2'$	500–680	464–662	183 and 184
89	NS	$C^2\Sigma^+ - X^2\Pi$	230–232	236–238	318
		NR	300–310, 360–370	*NR*	319
90	O_2 ††	$B^3\Sigma_u^- - X^3\Sigma_g^-$	223–226	240–440	135
91	OH‡	X – A	280–286	304–314	73, 75, and 144
92	PbF	$A^2\Sigma_{1/2}^+ - X_1^2\Pi_{1/2}$	260–285	*NR*	320 and 321
		$B^2\Sigma^+ - X^2\Pi_{1/2}$	426–450	435–500, 700–800, 1200–1300	322
93	P_2	*NR*	193	322.2	210
94	PH_2	$\tilde{A}^2A_1 - \tilde{X}^2B_1$	419–547	430–555	323–325
95	PO	$B^2\Sigma^+ - C^2\Pi$	324	*NR*	326
		$A^2\Sigma^+ - X^2\Pi_{1/2}$	245.6–246.6	239–279, 319–359	327
		$A^2\Sigma^+ - X^2\Pi_{3/2}$	247–247.8	239–279, 319–359	327
96	RuB	$[18.4]2.5 - X^2\Delta_{5/2}$	522–524, 542–543	*NR*	328
97	RuC	$[18.1]^1\Pi_1 - X^1\Pi^+, [5.7]^1\Delta_2$	431–439, 552.9	553, 806	329
98	RuCl	$^4\Gamma_{5.5} - X^4\phi_{4.5}$	508–557	499–546	185
		$^4\phi_{4.5} - X^4\phi_{4.5}$	426–569	430–442	
99	RuF	$[18.2]^4\Gamma_{4.5} - X^4\phi_{3.5}$	450–452	410–441	185
			545–548	470–533	
			758–764	697–732	
100	RuN	$(0,0)F^2\Sigma^+ - X^2\Sigma^+$	529.6–532	*NR*	330
101	RuO	$[18.1]4 - X^5\Delta_4$	529.5–531	463–503	185
102	SH	$^2\Sigma^+ - ^2\Pi_{3/2,1/2}$	323–330	320–362	165–167
103	SiBr	$B^2\Sigma - X^2\Pi_r$	308	296–304	147 and 331
104	SiCCl	$\tilde{A}^2\Sigma^+ - \tilde{X}^2\Pi$	550–615	545–650	197
105	SiCF	$\tilde{A}^2\Sigma^+ - \tilde{X}^2\Pi$	574–604	547–596	198
106	SiCH	$\tilde{A}^2\Sigma^+ - \tilde{X}^2\Pi_i$	650–680, 700–740	*NR*	332
107	SiCl	$B^2\,\Sigma - X^2\,\Pi$	275, 295, 308	280, 320, 290–307	146 and 147
108	$SiCl_2$	$\tilde{A}^1B_1 - \tilde{X}^1A_1$	309–333	331–390	333
109	$SiCl_3O$	$\tilde{A}^2A_1 - \tilde{X}^2E$	590–650	617–653	203
110	SiC_3H	$\tilde{A}^2\Sigma^+ - \tilde{X}^2\Pi_i$	613–681	578–663	204
111	SiF	X – B	288	308–315	148
112	SiF_2	X – A	221.6	234–244	148

03 December 2024 20:43:44

TABLE II. (Continued.)

Sl. No.	Species	Transition	Excitation (nm)	Fluorescence (nm)	Reference
113	SiH	$A^2\Delta - X^2\Pi$	409–416	413	45 and 334–336
114	SiH$_2$	$\tilde{A}\,^1B - \tilde{X}\,^1A$	579.2–580.4	618	337–339
115	SiN	$\tilde{B}\,^2\Sigma - \tilde{X}\,^2\Sigma$	396	414	175
116	SiO	$A\,^1\Sigma - X^1\Sigma$	220–237	214–350	48, 137, and 138
117	SO	NR	248.1, 248.7	250–450	340
118	SO$_2$	NR	248.1, 248.7	250–450	340
		$\tilde{X}(^1A_1) - \tilde{C}(^1B_2),\ \tilde{B}(^1B_1),\ \tilde{A}(^1A_2)$	266	250–350	341
119	S$_2$	$B^3\Sigma_u^- - X^3\Sigma_g^-$	325, 337	310–410	342
120	S$_2$O	$\tilde{C}\,^1A - \tilde{X}\,^1A$	340	NR	191 and 343
121	TaC	$[18.61]^2\Pi_{3/2} - X^2\Sigma^+$, NR	537.1–537.8, 505.2	401–509	344
122	TiC	$^1\Pi - X^3\Sigma^+$	606.9–608.3	538–603	199
		$^1\Pi - a^1\Sigma^+$	619.8–621.6	NR	
		$^1\Pi - b^1\Sigma^+$	690.4–691.5	NR	
		$^1\Pi - c^1\Sigma^+$	664.5–665.5	NR	
123	TiF	$[37.8]^4\Phi - X^4\Phi$	250.9–255.4	NR	345
		$^4\Delta - X^4\Phi$	249.5–250.1	NR	345

TABLE III. Laser-induced fluorescence transitions of neutral atomic species. NR, not reported. ‡: Absolute density reported.

Sl. No.	Species	Transition	Excitation (nm)	Fluorescence (nm)	Reference
1	Al	$^2P^0_{3/2} - ^2D_{5/2}$	309.3	394.4, 396.2	346
		$3^2P_{1/2} - 4^2S_{1/2}$	394.4	396.2	347
2	As	$4s^3\,^4S_{3/2} - 5s\,^4P_{3/2}$	193.8	245	348
3	B	$2s^22p\,^2P^0_{3/2} - 2s^23s\,^2S_{1/2}$	249.7, 249.8	209, 206.7	349
		$2s^22p\,^2P^0_{3/2} - 2s2p^2\,^2D_{3/2,5/2}$	208.96	208.96	350
4	Br	$4p^5\,^2P^0_{3/2} - 5p\,^4S^0_{3/2}$	2 × 252.59	635	351
5	C	$2p3p\,^3P - 2p^2\,^3P$	2 × 280	910	352
6	Cl‡	$3p^5\,^2P^0 - 4p\,^4S^0$	2 × 233.2	725–775	47, 353, and 354
7	Cr‡	$3d^54p^7P_J - 3d^54s^7S_3$	425.4	427.5, 429	355
8	Cu‡	$4s^2S_{1/2} - 4p^2P^0_{3/2}$	324.8	510.6, 570	356 and 357
9	F	$2p^5\,^2P^0 - 3p\,^2D^0$	170	776	46
10	Fe‡	$3d^64s^2a\,^5D_4 - 3d^7(^4F)4p\,y\,^5F^0_5$	296.7	373.5	358
		$3d^64s^2a\,^5D_4 - 3d^7(^4F)4p\,y\,^5D^0_4$	302.06	382.04	359
		$3d^6a^3F4s4p^3P^0 - 3d^64S^2$	225.15	248, 268, 300	360
11	Ga	$4^2D_{3/2} - 4^2P_{1/2}, 5^2S_{1/2} - 4^2P_{3/2}$	287.4, 403.3	294.4, 417.2	361
12	H‡	$1s^2S - 3d\,^2D$	2 × 205	656.3	66
13	I	$5p^5\,^2P^0 - ^2D^0$	2 × 304.7	178.3	362
14	Kr‡	$4p^6\,^1S_0 - 5p'[3/2]_2$	2 × 204.1	587, 826.3	66
15	N‡	$2p^3\,^4S^0 - 3p\,^4D^0$	2 × 206.6	870, 822, 744	66
16	Na‡	NR	2 × 685	818	363
		$^2P_{1/2}, ^2P_{3/2} - ^2S_{1/2}$	589	NR	364 and 365
17	O‡	$2p^4\,^3P - 3p\,^3P$	2 × 225.7	844.9, 777	66
18	Pb	$6s^26p^2\,^3P_0 - 6s^26p(2P^0_{0.5})7s\,3P^0_1$	283.31	405.78	366
19	S	$3p^4\,^3P - 4p\,^3P$	2 × 288	VUV	367
20	Si	$3p^2\,^3P_0 - 4s\,^3P^0_1$	251.4	252.8	368
21	Ti‡	$3d_2\,4s4p - 3d_2\,4s_2(^3F_3)$	322.3	511.3	369
		$^3D_{1,2,3}, ^1F_3, ^3F_3, ^3G_3 - ^3F_{2,3,4}$	221–296	250–341	145
22	W‡	$5d^46s^2\,^5D_0 - 5d^5\,^4D6s^0_1$	287.9	302.5	149 and 150
23	Xe‡	$5p^6\,^1S_0 - 7p[3/2]_2$	2 × 225.5	462.6	66

TABLE IV. Laser-induced fluorescence transitions of the metastable and ground states of ionic species.

Sl. No.	Species	Transition	Excitation (nm)	Fluorescence (nm)	Reference
1	Ar^{+*}	$3d^4\,F_{9/2} - 4p^4\,F_{7/2}$	664.4	434.8	370
		$3d^4\,F_{7/2} - 4p^4\,D_{5/2}$	668.6	442.7	102, 371–374, and 374–377
		$4p^2D_{5/2} - 4s^2P_{3/2}$	488	422.8	90
		$4p\,{}^2F^0_{7/2} - 3d'\,{}^2G_{9/2}$	611.7	461.1	378
2	Br_2^+	${}^2\Pi_u - X^2\Pi_g$	472.7	480–640	180
3	Cl^{+*}	${}^5P_3 - {}^5D_4^0$	542.3	479.5	379
4	Cl_2^+	$X^2\Pi_i - A^2\Pi_i$	387.6	396	380
5	CS_2^+	$X^2\Pi_{3/2} - A^2\Pi_{3/2}$	427–476	460–550	176
		$A^2\Pi_u - X^2\Pi_g$	410–480	507.7	381
6	$C_2S_2^-$	${}^2\Pi_{3/2} - {}^2\Pi_{3/2}$	542.5–543	555–695	382
7	I^{+*}	${}^5D_4^0 - {}^5P_3$	696.1	516.3	383
8	Kr^{+*}	$4d^4F_{7/2} -$	820.3	462.9	384
		$5d^4F_{7/2} -$	729	473.9	385
9	La^{+*}	$5d6s\,a^3D_1 - 5d6p\,y^3D_2^0$	403.2	379.1	386
10	N_2^+	$B^2\,\Sigma_u^+ - X^2\Sigma_g^+$	391	428	43
			330	458.8	387
11	N_2O^+	$\tilde{A}^2\Sigma^+ - \tilde{X}^2\Pi_i$	337–356	312–345	164
12	O_2^+	$X^2\Pi_g - A^2\Pi_u$	225–227	245	136
13	SiO^+	$B^2\Sigma^+ - X^2\Sigma^+$	385	383–385	388
14	Ti^+	$3d_2\,4p(z^4G^0_{5/2}) - 3d_2\,4s(a^4F_{3/2})$	338.4	486.6	369
15	Xe^{+*}	$5d^4F_{5/2} - 6p^4D_{5/2}$	834.7	541.9	59
		$6p^4P^0_{5/2} - 5d^4D_{7/2}$	605.1	529.2	389 and 390
		$6p^4D^0_{5/2} - 5d^4F_{7/2}$	680.6	492.2	44

IV. SUMMARY

Laser-induced fluorescence provides both spatial and temporally resolved characteristics of the neutral species, plasma-produced radicals, ions, and metastables. It is a useful tool that enables the direct measurement of densities, ion velocities, and temperatures. LIF can help in the validation of simulation models and help in the development of the predictive capabilities of plasma-material interactions. In this report, we have reviewed the basic principles of LIF, the widely used types of LIF setups, and compiled a list of the available transitions to generate a reference data for the laser-induced fluorescence transitions relevant in the microelectronics industry and the sustainability applications. We have identified the groups of

TABLE V. Laser-induced fluorescence transitions of neutral metastable species. ‡: Absolute density reported.

Sl. No.	Species	Transition	Excitation (nm)	Fluorescence (nm)	Reference
1	$Ar^{\star\,\ddagger}$	$3p^5P_{1/2} - 4p^5D_{3/2}$	696.7	826.7	51 and 101
		$3p^5S_{1/2} - 4p^5P_{1/2}$	772.6	810.6, 826.7	391
		$1s_5 - 2p_9$	811.5, 810.4	811.5, 772.6	392
		$1s_2 - 2p_3$	841.1	706.9	393
		$1s_2 - 2p_3$	842.5	842.5, 801.7	394
		$3d^4F_{(7/2)} - 4p^4D_{(3/2)}$	667.9	750.6	376 and 377
2	$F^{\star}$	${}^4D^0_{5/2} - {}^4P_{3/2}$	690.3	677.4	395
3	$He^{\star}$	$3^3P - 2^3S$	388.9	706.5, 587.6	396
		$2^1S - 3^1P$	501.6	667.8	396
4	$He^{\star}_2$	$a^3\Sigma_u^+ - d^3\Sigma_u^+$	2×940	640	397
5	$Kr^{\star}$	$5s[3/2]_2^0 - 5p[3/2]_2$	760.2	819	398 and 399
		$5s[3/2]_2 - 5p[5/2]_2$	810.44	877.6	398
6	$N_2^{\star}\,S^{\ddagger}$	$A^3\Sigma_u^+ - B^3\Pi_g$	687.44, 618	762, 676	400 and 401
7	$P^{\star}$	$3s^23p^3\,{}^2P^0_{1/2,3/2} - 3s^23p^2({}^3P)4s\,{}^2P_{3/2}$	253.4, 253.6	213.6, 213.6	402 and 403
8	$Xe^{\star}$	$6s^2[1/2]^0_1 - 6p^2[3/2]^0_1$	834.7	473.4	59 and 404
		$6s[3/2]^0_2 - 6p[3/2]_2$	823.2	823.2	404 and 405

species with overlapping LIF/TALIF excitations and fluorescence wavelengths. This compilation intends to assist in the identification of the possible species that can be detected by a LIF/TALIF interrogation volume. With the emergence of the use of new recipes for microelectronics and sustainability applications,[406] there is a need to explore previously unstudied species and LIF transitions that have not been previously explored. A central database with the required transition parameters for diagnostics such as LIF and absorption spectroscopy would be of immense value to the scientific community and these industrial applications.

AUTHOR DECLARATIONS

Conflict of Interest

The authors have no conflicts to disclose.

Author Contributions

V. S. Santosh K. Kondeti: Conceptualization (equal); Data curation (equal); Formal analysis (equal); Investigation (equal); Methodology (equal); Writing – original draft (equal); Writing – review & editing (equal). **Shurik Yatom:** Conceptualization (equal); Data curation (equal); Formal analysis (equal); Investigation (equal); Methodology (equal); Writing – original draft (equal); Writing – review & editing (equal). **Ivan Romadanov:** Conceptualization (equal); Data curation (equal); Formal analysis (equal); Investigation (equal); Methodology (equal); Writing – original draft (equal); Writing – review & editing (equal). **Yevgeny Raitses:** Conceptualization (equal); Data curation (equal); Formal analysis (equal); Funding acquisition (equal); Investigation (equal); Methodology (equal); Writing – original draft (equal); Writing – review & editing (equal). **Leonid Dorf:** Conceptualization (equal); Data curation (equal); Formal analysis (equal); Funding acquisition (equal); Investigation (equal); Methodology (equal); Writing – original draft (equal); Writing – review & editing (equal). **Andrei Khomenko:** Conceptualization (equal); Data curation (equal); Formal analysis (equal); Investigation (equal); Methodology (equal); Writing – original draft (equal); Writing – review & editing (equal).

DATA AVAILABILITY

Data sharing is not applicable to this article as no new data were created or analyzed in this study.

REFERENCES

[1] M. M. Waldrop, Nat. News **530**, 144 (2016).
[2] M. S. Lundstrom and M. A. Alam, Science **378**, 722 (2022).
[3] J. Shalf, Philos. Trans. R. Soc. A **378**, 20190061 (2020).
[4] T. N. Theis and H.-S. P. Wong, Comput. Sci. Eng. **19**, 41 (2017).
[5] D. B. Graves, IEEE Trans. Plasma Sci. **22**, 31 (1994).
[6] I. Adamovich et al. J. Phys. D: Appl. Phys. **55**, 373001 (2022).
[7] G. N. Parsons and R. D. Clark, Chem. Mater. **32**, 4920 (2020).
[8] H. C. Knoops, T. Faraz, K. Arts, and W. M. Kessels, J. Vac. Sci. Technol., A **37**, 030902 (2019).
[9] G. Oehrlein, D. Metzler, and C. Li, ECS J. Solid State Sci. Technol. **4**, N5041 (2015).
[10] L. Dorf, J.-C. Wang, S. Rauf, Y. Zhang, A. Agarwal, J. Kenney, K. Ramaswamy, and K. Collins, "Atomic precision etch using a low-electron temperature plasma," in Advanced Etch Technology for Nanopatterning V (SPIE, San Jose, CA, 2016), Vol. 9782, pp. 30–37.
[11] A. V. Jagtiani et al. J. Vac. Sci. Technol., A **34**, 01B103 (2016).
[12] S. Rauf, A. Balakrishna, A. Agarwal, L. Dorf, K. Collins, D. R. Boris, and S. G. Walton, Plasma Sources Sci. Technol. **26**, 065006 (2017).
[13] L. Dorf et al. Plasma processing assembly using pulsed-voltage and radio-frequency power," U.S. patent 11,462,388 (4 October 2022).
[14] L. Dorf, R. Dhindsa, J. Rogers, D. S. Byun, E. Kamenetskiy, Y. Guo, K. Ramaswamy, V. N. Todorow, and O. Luere, "Plasma processing using pulsed-voltage and radio-frequency power," U.S. patent application 17/315,234 (19 December 2023).
[15] L. Zhang, IEEE Consum. Electron. Mag. **3**, 44 (2014).
[16] K. Bera, S. Rauf, J. Forster, and K. Collins, J. Appl. Phys. **129**, 053304 (2021).
[17] G. Cunge, M. Kogelschatz, O. Joubert, and N. Sadeghi, Plasma Sources Sci. Technol. **14**, S42 (2005).
[18] M. Badaroglu, "International roadmap for devices and systems," More Moore https://irds.ieee.org/roadmap-2017 (2017).
[19] M. Atature, D. Englund, N. Vamivakas, S.-Y. Lee, and J. Wrachtrup, Nat. Rev. Mater. **3**, 38 (2018).
[20] F. A. Zwanenburg, A. S. Dzurak, A. Morello, M. Y. Simmons, L. C. Hollenberg, G. Klimeck, S. Rogge, S. N. Coppersmith, and M. A. Eriksson, Rev. Mod. Phys. **85**, 961 (2013).
[21] T. D. Ladd, F. Jelezko, R. Laflamme, Y. Nakamura, C. Monroe, and J. L. O'Brien, Nature **464**, 45 (2010).
[22] S. Samukawa et al. J. Phys. D: Appl. Phys. **45**, 253001 (2012).
[23] I. Adamovich et al. J. Phys. D: Appl. Phys. **50**, 323001 (2017).
[24] M. G. Kong, G. Kroesen, G. Morfill, T. Nosenko, T. Shimizu, J. Van Dijk, and J. Zimmermann, New J. Phys. **11**, 115012 (2009).
[25] P. Ranieri, N. Sponsel, J. Kizer, M. Rojas-Pierce, R. Hernández, L. Gatiboni, A. Grunden, and K. Stapelmann, Plasma Processes Polym. **18**, 2000162 (2021).
[26] Q. Chen, J. Li, and Y. Li, J. Phys. D: Appl. Phys. **48**, 424005 (2015).
[27] A. Bogaerts et al. J. Phys. D: Appl. Phys. **53**, 443001 (2020).
[28] J. C. Whitehead, J. Phys. D: Appl. Phys. **49**, 243001 (2016).
[29] A. Vardelle, C. Moreau, N. J. Themelis, and C. Chazelas, Plasma Chem. Plasma Process. **35**, 491 (2015).
[30] S. M. Starikovskaia, J. Phys. D: Appl. Phys. **39**, R265 (2006).
[31] Y. Huang, S. Li, Q. Zheng, X. Shen, S. Wang, P. Han, Z. Liu, and K. Yan, Int. J. Plasma Environ. Sci. Technol. **9**, 69 (2015).
[32] S. Nijdam, E. Van Veldhuizen, P. Bruggeman, and U. Ebert, "An introduction to nonequilibrium plasmas at atmospheric pressure," in Plasma Chemistry and Catalysis in Gases and Liquids, edited by V. I. Parvulescu, M. Magureanu, and P. Lukes (John Wiley and Sons, New York, 2012), pp. 1–44.
[33] Y.-S. Byeon, E. J. Hong, S. Yoo, T. Lho, S.-Y. Yoon, S. B. Kim, S. J. Yoo, and S. Ryu, Plasma Chem. Plasma Process. **37**, 1405 (2017).
[34] G. Trenchev and A. Bogaerts, J. CO2 Util. **39**, 101152 (2020).
[35] Y. Sui, C. A. Zorman, and R. M. Sankaran, Plasma Processes Polym. **17**, 2000009 (2020).
[36] P. J. Bruggeman et al. Plasma Sources Sci. Technol. **25**, 053002 (2016).
[37] G. S. Oehrlein, R. J. Phaneuf, and D. B. Graves, J. Vac. Sci. Technol., B **29**, 010801 (2011).
[38] K. Becker, K. Schoenbach, and J. Eden, J. Phys. D: Appl. Phys. **39**, R55 (2006).
[39] Y. Kusano, J. Adhes. **90**, 755 (2014).

03 December 2024 20:43:44

[40]J. Amorim, G. Baravian, and J. Jolly, J. Phys. D: Appl. Phys. **33**, R51 (2000).

[41]H. Döbele, T. Mosbach, K. Niemi, and V. Schulz-Von Der Gathen, Plasma Sources Sci. Technol. **14**, S31 (2005).

[42]V. Donnelly, D. Flamm, and G. Collins, J. Vac. Sci. Technol. **21**, 817 (1982).

[43]K. Konthasinghe, K. Fitzmorris, M. Peiris, A. J. Hopkins, B. Petrak, D. K. Killinger, and A. Muller, Appl. Spectrosc. **69**, 1042 (2015).

[44]D. Lee, N. Hershkowitz, and G. D. Severn, Appl. Phys. Lett. **91**, 041505 (2007).

[45]K. Tachibana, T. M. T. Mukai, and H. H. H. Harima, Jpn. J. Appl. Phys. **30**, L1208 (1991).

[46]G. Herring, M. J. Dyer, L. E. Jusinski, and W. K. Bischel, Opt. Lett. **13**, 360 (1988).

[47]G. S. Selwyn, L. Baston, and H. Sawin, Appl. Phys. Lett. **51**, 898 (1987).

[48]P. van de Weijer and B. H. Zwerver, Chem. Phys. Lett. **163**, 48 (1989).

[49]A. Diallo, S. Keller, Y. Shi, Y. Raitses, and S. Mazouffre, Rev. Sci. Instrum. **86**, 033506 (2015).

[50]P. J. Bruggeman, N. Sadeghi, D. Schram, and V. Linss, Plasma Sources Sci. Technol. **23**, 023001 (2014).

[51]S. Yatom, N. Chopra, S. Kondeti, T. B. Petrova, Y. Raitses, D. R. Boris, M. J. Johnson, and S. G. Walton, Plasma Sources Sci. Technol. **32**, 115005 (2023).

[52]R. Forster, M. Frost, D. Fulle, H. Hamann, H. Hippler, A. Schlepegrell, and J. Troe, J. Chem. Phys. **103**, 2949 (1995).

[53]M. Mrkvičková, P. Dvořák, M. Svoboda, J. Kratzer, J. Voráč, and J. Dědina, Combust. Flame **241**, 112100 (2022).

[54]M. Goeckner, J. Goree, and T. Sheridan, Rev. Sci. Instrum. **64**, 996 (1993).

[55]S. Mazouffre, "Laser-induced fluorescence spectroscopy applied to electric thrusters," in *Von Karman Institute for Fluid Dynamics STO-AVT-VKI Lecture series 263*, edited by T. Magin (HAL Open Science, 2016); available at https://hal.science/hal-03576139v1.

[56]V. Kondeti, Y. Zheng, P. Luan, G. S. Oehrlein, and P. J. Bruggeman, J. Vac. Sci. Technol., A **38**, 033012 (2020).

[57]S. Yatom, Y. Luo, Q. Xiong, and P. J. Bruggeman, J. Phys. D: Appl. Phys. **50**, 415204 (2017).

[58]V. Kondeti, U. Gangal, S. Yatom, and P. J. Bruggeman, J. Vac. Sci. Technol., A **35**, 061302 (2017).

[59]P. Svarnas, I. Romadanov, A. Diallo, and Y. Raitses, IEEE Trans. Plasma Sci. **46**, 3998 (2018).

[60]L. Pietzonka, C. Eichhorn, F. Scholze, and D. Spemann, J. Electr. Propul. **2**, 4 (2023).

[61]A. E. Vinci, S. Mazouffre, V. Gómez, P. Fajardo, and J. Navarro-Cavallé, Plasma Sources Sci. Technol. **31**, 095007 (2022).

[62]C. Brackmann, B. Zhou, Z. Li, and M. Alden, Combust. Sci. Technol. **188**, 529 (2016).

[63]A. Hirano and M. Tsujishita, Appl. Opt. **33**, 7777 (1994).

[64]B. J. Kirby and B. K. Hanson, Proc. Combust. Inst. **28**, 253 (2000).

[65]A. D. Sappey and T. K. Gamble, J. Appl. Phys. **72**, 5095 (1992).

[66]K. Niemi, V. Schulz-Von Der Gathen, and H. Döbele, J. Phys. D: Appl. Phys. **34**, 2330 (2001).

[67]W. D. Kulatilaka, J. H. Frank, and T. B. Settersten, Proc. Combust. Inst. **32**, 955 (2009).

[68]A. Dogariu, E. Evans, S. P. Vinoth, and S. A. Cohen, "Non-invasive neutral atom density measurements using fs-TALIF in a magnetic linear plasma device," in *CLEO: Science and Innovations* (Optica Publishing Group, San Jose, CA, 2021), pp. SM1E-1.

[69]S. Yatom and D. Dobrynin, J. Phys. D: Appl. Phys. **55**, 485203 (2022).

[70]F. Träger, *Springer Handbook of Lasers and Optics* (Springer, New York, 2012), Vol. 2.

[71]K. F. Renk, *Basics of Laser Physics* (Springer, New York, 2012).

[72]V. Vekselman, J. Gleizer, S. Yatom, V. T. Gurovich, and Y. E. Krasik, J. Appl. Phys. **108**, 093303 (2010).

[73]T. Verreycken, R. Mensink, R. Van Der Horst, N. Sadeghi, and P. J. Bruggeman, Plasma Sources Sci. Technol. **22**, 055014 (2013).

[74]R. B. Miles, W. R. Lempert, and J. N. Forkey, Meas. Sci. Technol. **12**, R33 (2001).

[75]T. Verreycken, R. Van Der Horst, N. Sadeghi, and P. J. Bruggeman, J. Phys. D: Appl. Phys. **46**, 464004 (2013).

[76]W. Kauzmann, *Kinetic Theory of Gases* (Courier Corporation, New York, 2012).

[77]G. J. Fiechtner and J. R. Gord, J. Quant. Spectrosc. Radiat. Transfer **68**, 543 (2001).

[78]H. Ludvigsen, M. Tossavainen, and M. Kaivola, Opt. Commun. **155**, 180 (1998).

[79]J. Reid, D. Cassidy, and R. Menzies, Appl. Opt. **21**, 3961 (1982).

[80]J. Luque and D. Crosley, Appl. Phys. B **63**, 91 (1996).

[81]S. Nemschokmichal and J. Meichsner, Plasma Sources Sci. Technol. **22**, 015005 (2012).

[82]D. H. Campbell, Appl. Opt. **23**, 689 (1984).

[83]D. H. Campbell, Appl. Opt. **23**, 1319 (1984).

[84]A. Kramida, Yu. Ralchenko, J. Reader, and NIST ASD Team, "NIST atomic spectra database (ver. 5.11), (Online), available at: https://physics.nist.gov/asd [2024, June 1] (National Institute of Standards and Technology, Gaithersburg, 2024).

[85]K. Huber, *Molecular Spectra and Molecular Structure: IV. Constants of Diatomic Molecules* (Springer Science & Business Media, Berlin, 2013).

[86]C. Kaminski and P. Ewart, Appl. Phys. B **61**, 585 (1995).

[87]J. Luque, W. Juchmann, and J. Jeffries, J. Appl. Phys. **82**, 2072 (1997).

[88]A. Van Gessel, B. Hrycak, M. Jasiński, J. Mizeraczyk, J. Van Der Mullen, and P. Bruggeman, J. Phys. D: Appl. Phys. **46**, 095201 (2013).

[89]J. B. Schmidt, "Ultrashort two-photon-absorption laser-induced fluorescence in nanosecond-duration, repetitively pulsed discharges," Ph.D. thesis (The Ohio State University, 2015).

[90]R. Stern and J. Johnson III, Phys. Rev. Lett. **34**, 1548 (1975).

[91]V. Vekselman, J. Gleizer, S. Yatom, D. Yarmolich, V. T. Gurovich, G. Bazalitski, Y. E. Krasik, and V. Bernshtam, Phys. Plasmas **16**, 113504 (2009).

[92]V. Gavrilenko, H. Kim, T. Ikutake, J. Kim, Y. Choi, M. Bowden, and K. Muraoka, Phys. Rev. E **62**, 7201 (2000).

[93]B. B. Ngom, T. B. Smith, W. Huang, and A. D. Gallimore, J. Appl. Phys. **104**, 023303 (2008).

[94]J. Pérez-Luna, G. J. M. Hagelaar, L. Garrigues, and J. P. Boeuf, Plasma Sources Sci. Technol. **18**, 034008 (2009).

[95]C. Cohen-Tannoudji, B. Diu, and F. Laloë, *Quantum Mechanics Volume 1* (Hermann, Paris, 1977).

[96]I. Romadanov, Y. Raitses, A. Diallo, K. Hara, I. Kaganovich, and A. Smolyakov, Phys. Plasmas **25**, 033501 (2018).

[97]S. Mazouffre, Plasma Sources Sci. Technol. **22**, 013001 (2012).

[98]V. Chaplin, R. Lobbia, A. Lopez Ortega, I. Mikellides, R. Hofer, J. Polk, and A. Friss, Appl. Phys. Lett. **116**, 234107 (2020).

[99]J. Vaudolon, B. Khiar, and S. Mazouffre, Plasma Sources Sci. Technol. **23**, 022002 (2014).

[100]C. V. Young, A. L. Fabris, N. A. MacDonald-Tenenbaum, W. A. Hargus, and M. A. Cappelli, Plasma Sources Sci. Technol. **27**, 094004 (2018).

[101]M. Aramaki, K. Ogiwara, S. Etoh, S. Yoshimura, and M. Y. Tanaka, Rev. Sci. Instrum. **80**, 053505 (2009).

[102]R. Boivin and E. Scime, Rev. Sci. Instrum. **74**, 4352 (2003).

[103]W. Huang, T. Smith, and A. Gallimore, "Obtaining velocity distribution using a xenon ion line with unknown hyperfine constants," in *40th AIAA Plasmadynamics and Lasers Conference*, San Antonio, Texas, 22–25 June 2009 (AIAA, 2009), p. 4226.

[104]H.-J. Kunze, *Introduction to Plasma Spectroscopy* (Springer Science & Business Media, Berlin, 2009), Vol. 56.

[105]S. Hübner, N. Sadeghi, E. Carbone, and J. Van Der Mullen, J. Appl. Phys. **113**, 143306 (2013).

[106]E. Scime, C. Biloiu, C. Compton, F. Doss, D. Venture, J. Heard, E. Choueiri, and R. Spektor, Rev. Sci. Instrum. **76**, 026107 (2005).

[107]B. Pelissier and N. Sadeghi, Rev. Sci. Instrum. **67**, 3405 (1996).

[108]J. Vaudolon, L. Balika, and S. Mazouffre, Rev. Sci. Instrum. **84**, 073512 (2013).

[109]B. Jacobs, W. Gekelman, P. Pribyl, M. Barnes, and M. Kilgore, Appl. Phys. Lett. **91**, 161505 (2007).

[110]I. Romadanov, Y. Raitses, and A. Smolyakov, "Wavelength modulation laser-induced fluorescence for plasma characterization," arXiv:2403.11045 (2024).

[111]L. Dixit and S. Ram, Appl. Spectrosc. Rev. **21**, 311 (1985).

[112]F. Marchal, N. Sewraj, J.-P. Gardou, N. Merbahi, and M. Yousfi, "Study of formation and decay of rare-gas excimers by laser-induced fluorescence," in *Photon Counting—Fundamentals and Applications* (InTech, London, 2018).

[113]W. Amos and J. White, Biol. Cell **95**, 335 (2003).

[114]R. VanDervort, D. Elliott, D. McCarren, J. McKee, M. Soderholm, S. Sears, and E. Scime, Rev. Sci. Instrum. **85**, 11E408 (2014).

[115]D. S. Thompson, M. F. Henriquez, E. E. Scime, and T. N. Good, Rev. Sci. Instrum. **88**, 103506 (2017).

[116]T. Kajiwara, K. Takeda, K. Muraoka, T. Okada, M. Maeda, and M. Akazaki, Jpn. J. Appl. Phys. **29**, L826 (1990).

[117]D. Caron, R. John, E. Scime, and T. Steinberger, J. Vac. Sci. Technol., A **41**, 033001 (2023).

[118]I. Romadanov and Y. Raitses, Rev. Sci. Instrum. **94**, 073002 (2023).

[119]J. Lee, A. Efremov, and K.-H. Kwon, Vacuum **148**, 214 (2018).

[120]M. Foad, C. Wilkinson, C. Dunscomb, and R. Williams, Appl. Phys. Lett. **60**, 2531 (1992).

[121]F. Bell, O. Joubert, G. Oehrlein, Y. Zhang, and D. Vender, J. Vac. Sci. Technol., A **12**, 3095 (1994).

[122]X. Li, X. Hua, L. Ling, G. S. Oehrlein, M. Barela, and H. M. Anderson, J. Vac. Sci. Technol., A **20**, 2052 (2002).

[123]S.-W. Cho, C.-K. Kim, J.-K. Lee, S. H. Moon, and H. Chae, J. Vac. Sci. Technol., A **30**, 051301 (2012).

[124]H. Rhee, C. Kim, C.-K. Kim, H. Kim, J. Yoo, and Y. W. Kim, J. Vac. Sci. Technol., B **26**, 576 (2008).

[125]R. d'Agostino and D. L. Flamm, J. Appl. Phys. **52**, 162 (1981).

[126]A. Efremov, V. Betelin, and K.-H. Kwon, Russ. Microelectron. **49**, 379 (2020).

[127]J. K. Kim, S. I. Cho, N. G. Kim, M. S. Jhon, K. S. Min, C. K. Kim, and G. Y. Yeom, J. Vac. Sci. Technol., A **31**, 021301 (2013).

[128]L. Jiang, N. Plank, M. Blauw, R. Cheung, and E. van der Drift, J. Phys. D: Appl. Phys. **37**, 1809 (2004).

[129]V. M. Donnelly, D. L. Flamm, W. Dautremont-Smith, and D. Werder, J. Appl. Phys. **55**, 242 (1984).

[130]H. Nishino, N. Hayasaka, and H. Okano, J. Appl. Phys. **74**, 1345 (1993).

[131]M. M. Hefny, C. Pattyn, P. Lukes, and J. Benedikt, J. Phys. D: Appl. Phys. **49**, 404002 (2016).

[132]S. Yatom, Phys. Plasmas **30**, 033507 (2023).

[133]C. Brackmann, J. Bood, J. D. Naucler, A. A. Konnov, and M. Alden, Proc. Combust. Inst. **36**, 4533 (2017).

[134]M. P. Lee, B. K. McMillin, and R. K. Hanson, Appl. Opt. **32**, 5379 (1993).

[135]J. Goldsmith and R. Anderson, Opt. Lett. **11**, 67 (1986).

[136]J. Li, V. M. Bierbaum, and S. R. Leone, Chem. Phys. Lett. **330**, 331 (2000).

[137]R. S. Chrystie, O. M. Feroughi, T. Dreier, and C. Schulz, Appl. Phys. B **123**, 1 (2017).

[138]R. S. Chrystie, F. L. Ebertz, T. Dreier, and C. Schulz, Appl. Phys. B **125**, 1 (2019).

[139]D. Gutman, N. Sanders, and J. Butler, J. Phys. Chem. **86**, 66 (1982).

[140]T. Ebata, H. Yanagishita, K. Obi, and I. Tanaka, Chem. Phys. **69**, 27 (1982).

[141]G. Inoue, H. Akimoto, and M. Okuda, Chem. Phys. Lett. **63**, 213 (1979).

[142]G. Inoue, H. Akimoto, and M. Okuda, J. Chem. Phys. **72**, 1769 (1980).

[143]J. Kappert and F. Temps, Chem. Phys. **132**, 197 (1989).

[144]A. M. Irvine, I. W. Smith, R. P. Tuckett, and X.-F. Yang, J. Chem. Phys. **93**, 3177 (1990).

[145]P. Ljung, E. Nyström, J. Enger, P. Ljungberg, and O. Axner, Spectrochim. Acta, Part B **52**, 675 (1997).

[146]S. Singleton, K. G. McKendrick, R. A. Copeland, and J. B. Jeffries, J. Phys. Chem. **96**, 9703 (1992).

[147]I. P. Herman, V. M. Donnelly, C.-C. Cheng, and K. V. Guinn, Jpn. J. Appl. Phys. **35**, 2410 (1996).

[148]G. Hebner, J. Appl. Phys. **90**, 4938 (2001).

[149]S. Hadrath, J. Ehlbeck, G. Lieder, and F. Sigeneger, J. Phys. D: Appl. Phys. **38**, 3285 (2005).

[150]A. Georgiev, A. Blagoev, and A. Pashov, AIP Conf. Proc. **2075**, 050005 (2019).

[151]M.-C. Yang, J. Williamson, and T. A. Miller, J. Mol. Spectrosc. **186**, 1 (1997).

[152]Z. Li and J. Francisco, Chem. Phys. Lett. **186**, 336 (1991).

[153]J. A. Sutton, B. A. Williams, and J. W. Fleming, Combust. Flame **153**, 465 (2008).

[154]G. P. Smith, R. A. Copeland, and D. R. Crosley, J. Chem. Phys. **91**, 1987 (1989).

[155]M. Curtis, A. Levick, and P. Sarre, Laser Chem. **9**, 359 (1988).

[156]G. Inoue and H. Akimoto, J. Chem. Phys. **74**, 425 (1981).

[157]K. Kleinermanns and A. Luntz, J. Phys. Chem. **85**, 1966 (1981).

[158]L. DiMauro, M. Heaven, and T. A. Miller, J. Chem. Phys. **81**, 2339 (1984).

[159]G. Inoue, M. Okuda, and H. Akimoto, J. Chem. Phys. **75**, 2060 (1981).

[160]G. Inoue and M. Suzuki, J. Chem. Phys. **84**, 3709 (1986).

[161]G. Wang, S. Wang, and T. F. Guiberti, Combust. Flame **256**, 112981 (2023).

[162]R. A. Copeland, M. L. Wise, K. J. Rensberger, and D. R. Crosley, Appl. Opt. **28**, 3199 (1989).

[163]H. Umemoto and K.-I. Matsumoto, J. Chem. Phys. **104**, 9640 (1996).

[164]M. A. Gharaibeh and D. J. Clouthier, J. Chem. Phys. **136**, 044318 (2012).

[165]J. Tiee, F. Wampler, R. Oldenborg, and W. Rice, Chem. Phys. Lett. **82**, 80 (1981).

[166]W. Hawkins and P. Houston, J. Chem. Phys. **73**, 297 (1980).

[167]K. Becker, D. Haaks, and T. Tatarczyk, Ber. Bunsen Ges. Phys. Chem. Chem. Phys. **78**, 1157 (1974).

[168]C. Brackmann, Z. Li, M. Rupinski, N. Docquier, G. Pengloan, and M. Aldén, Appl. Spectrosc. **59**, 763 (2005).

[169]J. E. Harrington and K. C. Smyth, Chem. Phys. Lett. **202**, 196 (1993).

[170]C. Conley, J. B. Halpern, J. Wood, C. Vaughn, and W. M. Jackson, Chem. Phys. Lett. **73**, 224 (1980).

[171]R. Cody, M. J. Sabety-Dzvonik, and W. Jackson, J. Chem. Phys. **66**, 2145 (1977).

[172]P. Bonczyk and J. Shirley, Combust. Flame **34**, 253 (1979).

[173]G. Black and L. E. Jusinski, Chem. Phys. Lett. **136**, 241 (1987).

[174]G. Black and L. E. Jusinski, Chem. Phys. Lett. **139**, 431 (1987).

[175]R. Walkup, P. Avouris, R. Dreyfus, J. Jasinski, and G. Selwyn, Appl. Phys. Lett. **45**, 372 (1984).

[176]V. Bondybey, J. English, and T. A. Miller, J. Chem. Phys. **70**, 1621 (1979).

[177]M. Nakajima, Y. Yoneda, H. Toyoshima, Y. Sumiyoshi, and Y. Endo, J. Mol. Spectrosc. **232**, 255 (2005).

[178]H. U. Lee and J. P. Deneufville, Chem. Phys. Lett. **99**, 394 (1983).

[179]R. Dixon and N. Wright, Chem. Phys. Lett. **117**, 280 (1985).

[180]T. Harris, J. Eland, and R. Tuckett, J. Mol. Spectrosc. **98**, 269 (1983).

[181]F. X. Sunahori, X. Zhang, and D. J. Clouthier, J. Chem. Phys. **125**, 084310 (2006).

[182]W. Demtröder, M. McClintock, and R. Zare, J. Chem. Phys. **51**, 5495 (1969).

[183]B. Kim, P. L. Hunter, and H. Johnston, J. Chem. Phys. **96**, 4057 (1992).

[184]M. Fukushima, J. Mol. Spectrosc. **387**, 111646 (2022).

[185]H. Zarringhalam, "High-resolution laser and far-infrared Fourier transform synchrotron-based spectroscopy of selected molecules," Ph.D. thesis (University of New Brunswick, 2022).

[186]K. Weyer, R. Beaudet, R. Straubinger, and H. Walther, Chem. Phys. **47**, 171 (1980).

[187]C. Focsa, H. Li, and P. Bernath, J. Mol. Spectrosc. **200**, 104 (2000).

[188]S. Bullman, J. Farthing, and J. Whitehead, Mol. Phys. **44**, 97 (1981).

[189]J. Danon, S. Filseth, D. Feldmann, H. Zacharias, C. Dugan, and K. Welge, Chem. Phys. **29**, 345 (1978).

[190]W. Pitts, V. Donnelley, A. Baronavski, and J. McDonald, Chem. Phys. **61**, 451 (1981).

[191]D. R. Crosley, High Temp. Mater. Processes **7**, 41 (1986).

[192]S. Mayama, K. Egashira, and K. Obi, Res. Chem. Intermed. **12**, 285 (1989).

[193]N. R. Taylor and K. M. Lemmer, J. Ionic Liq. **4**, 100084 (2024).

[194]R. A. Copeland, D. R. Crosley, and G. P. Smith, Symp. (Int.) Combust. **20**, 1195 (1985).

[195]J. Halpern, G. Hancock, M. Lenzi, and K. Welge, J. Chem. Phys. **63**, 4808 (1975).

[196]G. Hancock, W. Lange, M. Lenzi, and K. Welge, Chem. Phys. Lett. **33**, 168 (1975).

[197]G. Rothschopf, T. C. Smith, and D. J. Clouthier, J. Mol. Spectrosc. **359**, 22 (2019).

[198]G. Rothschopf, T. C. Smith, and D. J. Clouthier, J. Chem. Phys. **149**, 024301 (2018).

[199]S. Nakhate, S. Mukund, and S. Bhattacharyya, Chem. Phys. Lett. **680**, 51 (2017).

[200]F. X. Sunahori, J. Wei, and D. J. Clouthier, J. Chem. Phys. **128**, 244311 (2008).

[201]A. Schoeffler, H. Kohguchi, K. Hoshina, Y. Ohshima, and Y. Endo, J. Chem. Phys. **114**, 6142 (2001).

[202]F. X. Sunahori and D. J. Clouthier, J. Chem. Phys. **130**, 164310 (2009).

[203]T. C. Smith and D. J. Clouthier, J. Chem. Phys. **152**, 194303 (2020).

[204]H. Umeki, M. Nakajima, and Y. Endo, J. Chem. Phys. **143**, 174304 (2015).

[205]A. Colibaba-Evulet, A. Singhal, and N. Glumac, Combust. Sci. Technol. **157**, 129 (2000).

[206]K. Honma, J. Chem. Phys. **119**, 3641 (2003).

[207]J. Li, M. Xu, X. Li, Q. Ma, N. Zhao, Q. Zhang, L. Guo, and Y. Lu, Laser Phys. Lett. **16**, 055701 (2019).

[208]M. He, H. Wang, and B. R. Weiner, Chem. Phys. Lett. **204**, 563 (1993).

[209]A. L. Alstrin, R. V. Smilgys, P. G. Strupp, and S. R. Leone, J. Chem. Phys. **97**, 6864 (1992).

[210]V. Donnelly and R. Karlicek, J. Appl. Phys. **53**, 6399 (1982).

[211]R. V. Smilgys and S. R. Leone, J. Vac. Sci. Technol., B **8**, 416 (1990).

[212]Y. Ng, H. Pang, and A.-C. Cheung, Chem. Phys. Lett. **509**, 16 (2011).

[213]F. X. Sunahori, R. Nagarajan, and D. J. Clouthier, J. Chem. Phys. **143**, 224308 (2015).

[214]C. Fleddermann and G. Hebner, J. Appl. Phys. **83**, 4030 (1998).

[215]J. Rice, N. Caldwell, and H. Nelson, J. Phys. Chem. **93**, 3600 (1989).

[216]J. Harrison, R. Meads, and L. Phillips, Chem. Phys. Lett. **150**, 299 (1988).

[217]F. X. Sunahori, M. Gharaibeh, D. J. Clouthier, and R. Tarroni, J. Chem. Phys. **142**, 174302 (2015).

[218]M. A. Clyne and M. C. Heaven, Chem. Phys. **51**, 299 (1980).

[219]P. Maksyutenko, D. S. Parker, F. Zhang, and R. I. Kaiser, Rev. Sci. Instrum. **82**, 083107 (2011).

[220]G. R. Schneider and W. B. Roh, AIP Conf. Proc. **172**, 753 (1988).

[221]S.-G. He, C. J. Evans, and D. J. Clouthier, J. Chem. Phys. **119**, 2047 (2003).

[222]M. Nakajima, T. W. Schmidt, Y. Sumiyoshi, and Y. Endo, Chem. Phys. Lett. **449**, 57 (2007).

[223]S. Zhou, M. Zhan, J. Shi, and C. Wang, Chem. Phys. Lett. **166**, 547 (1990).

[224]C.-L. Lee, M.-L. Liu, and B.-C. Chang, Phys. Chem. Chem. Phys. **5**, 3859 (2003).

[225]W. Hack, Int. Rev. Phys. Chem. **4**, 165 (1985).

[226]J. Tiee, F. Wampler, and W. Rice, Jr., Chem. Phys. Lett. **73**, 519 (1980).

[227]R. Huie, N. Long, and B. Thrush, Chem. Phys. Lett. **51**, 197 (1977).

[228]N. D. Gómez, V. D'accurso, V. M. Freytes, F. A. Manzano, J. Codnia, and M. L. Azcárate, Int. J. Chem. Kinet. **45**, 306 (2013).

[229]Y. Liu, Y. Xin, L. Pei, Y. Chen, and C. Chen, Chem. Phys. Lett. **385**, 314 (2004).

[230]Q. Lu *et al.*, Chem. Phys. Lett. **178**, 517 (1991).

[231]J. Tiee, F. Wampler, and W. Rice, Chem. Phys. Lett. **65**, 425 (1979).

[232]J. S. Guss, C. A. Richmond, K. Nauta, and S. H. Kable, Phys. Chem. Chem. Phys. **7**, 100 (2005).

[233]M. Ludwiczak, D. Latimer, and R. Steer, J. Mol. Spectrosc. **147**, 414 (1991).

[234]J. Booth, G. Hancock, N. Perry, and M. Toogood, J. Appl. Phys. **66**, 5251 (1989).

[235]J. P. Barz, C. Oehr, and A. Lunk, Plasma Processes Polym. **8**, 409 (2011).

[236]D. S. King, P. K. Schenck, and J. C. Stephenson, J. Mol. Spectrosc. **78**, 1 (1979).

[237]B. K. McMillin and M. R. Zachariah, J. Vac. Sci. Technol., A **15**, 230 (1997).

[238]L. Rubio, M. Santos, and J. Torresano, J. Photochem. Photobiol., A **146**, 1 (2001).

[239]J. Purdy and B. Thrush, Chem. Phys. Lett. **73**, 228 (1980).

[240]B. S. Truscott, N. L. Elliott, and C. M. Western, J. Chem. Phys. **130**, 234301 (2009).

[241]J. S. Guss, O. Votava, and S. H. Kable, J. Chem. Phys. **115**, 11118 (2001).

[242]G. A. Raiche and J. B. Jeffries, Appl. Opt. **32**, 4629 (1993).

[243]J. Luque, W. Juchmann, and J. Jeffries, Appl. Opt. **36**, 3261 (1997).

[244]M. Engelhard, W. Jacob, W. Möller, and A. Koch, Appl. Opt. **34**, 4542 (1995).

[245]J. Luque, R. Klein-Douwel, J. Jeffries, G. Smith, and D. Crosley, Appl. Phys. B **75**, 779 (2002).

[246]K. Hakuta, J. Mol. Spectrosc. **106**, 56 (1984).

[247]D. L'Espérance, B. A. Williams, and J. W. Fleming, Chem. Phys. Lett. **280**, 113 (1997).

[248]M. Kakimoto, S. Saito, and E. Hirota, J. Mol. Spectrosc. **88**, 300 (1981).

[249]Y. Qiu, S. Zhou, and J. Shi, Chem. Phys. Lett. **136**, 93 (1987).

[250]M. N. Ashfold, F. Castano, G. Hancock, and G. Ketley, Chem. Phys. Lett. **73**, 421 (1980).

[251]G. Hancock and G. W. Ketley, J. Chem. Soc., Faraday Trans. 2 **78**, 1283 (1982).

[252]T. W. Schmidt, G. B. Bacskay, and S. H. Kable, J. Chem. Phys. **110**, 11277 (1999).

[253]L. Zu, J. Liu, G. Tarczay, P. Dupré, and T. A. Miller, J. Chem. Phys. **120**, 10579 (2004).

[254]M. Suzuki, G. Inoue, and H. Akimoto, J. Chem. Phys. **81**, 5405 (1984).

[255]G. Black and L. E. Jusinski, J. Chem. Soc., Faraday Trans. 2 **82**, 2143 (1986).

[256]B. Dally, A. Masri, R. Barlow, and G. Fiechtner, Combust. Flame **132**, 272 (2003).

[257]M. A. Damen, D. Hage, A. W. van de Steeg, L. M. Martini, and R. Engeln, Plasma Sources Sci. Technol. **28**, 115006 (2019).

[258]J. Zetterberg, S. Blomberg, J. Gustafson, Z. Sun, Z. Li, E. Lundgren, and M. Aldén, Rev. Sci. Instrum. **83**, 053104 (2012).

[259]Z. Alwahabi, J. Zetterberg, Z. Li, and M. Aldén, Eur. Phys. J. D **42**, 41 (2007).

[260]P. Clough and J. Johnston, Chem. Phys. Lett. **71**, 253 (1980).

[261]A. J. Hynes and J. H. Brophy, Chem. Phys. Lett. **63**, 93 (1979).

[262]M. Martin and R. J. Donovan, J. Photochem. **18**, 245 (1982).

[263]N. Ochi, H. Watanabe, S. Tsuchiya, and S. Koda, Chem. Phys. **113**, 271 (1987).

[264]T. Weyh and W. Demtröder, J. Chem. Phys. **104**, 6938 (1996).

[265]E. Martínez, M. López, J. Albaladejo, and F. Poblete, J. Mol. Struct. **408**, 553 (1997).

[266]W. N. Sisk, N. Sarkar, S. Ikeda, and H. Hayashi, J. Phys. Chem. A **103**, 7179 (1999).

[267]R. Dreyfus, J. Appl. Phys. **69**, 1721 (1991).

[268]V. Vekselman, A. Khrabry, I. Kaganovich, B. Stratton, R. Selinsky, and Y. Raitses, Plasma Sources Sci. Technol. **27**, 025008 (2018).

[269]H. Reisler, M. Mangir, and C. Wittig, Chem. Phys. **47**, 49 (1980).

[270]W. M. Pitts, L. Pasternack, and J. McDonald, Chem. Phys. **68**, 417 (1982).

[271]D. Jones and J. Mackie, Combust. Flame **27**, 143 (1976).

[272]T. Tatarczyk, E. Fink, and K. Becker, Chem. Phys. Lett. **40**, 126 (1976).

[273]B. Williams and J. Fleming, Appl. Phys. B **75**, 883 (2002).

[274]M. Nakajima, A. Miyoshi, Y. Sumiyoshi, and Y. Endo, J. Chem. Phys. **126**, 044307 (2007).

[275]W.-C. Hung, M.-Y. Shen, C.-H. Yu, and Y.-P. Lee, J. Chem. Phys. **105**, 5722 (1996).

[276]M. Kakimoto and T. Kasuya, J. Mol. Spectrosc. **94**, 380 (1982).

[277]K. Hakuta and H. Uehara, J. Chem. Phys. **78**, 6484 (1983).

[278]T. Ikegami, S. Ishibashi, Y. Yamagata, K. Ebihara, R. Thareja, and J. Narayan, J. Vac. Sci. Technol., A **19**, 1304 (2001).

[279]K. Hoshina and Y. Endo, J. Chem. Phys. **127**, 184304 (2007).

[280]K. Hoshina, H. Kohguchi, Y. Ohshima, and Y. Endo, J. Chem. Phys. **108**, 3465 (1998).

[281]B. A. Williams and J. W. Fleming, J. Chem. Phys. **106**, 4376 (1997).

[282]R. Callaghan, Y.-L. Huang, S. Arepalli, and R. J. Gordon, Chem. Phys. Lett. **158**, 531 (1989).

[283]R. König and J. Lademann, Chem. Phys. Lett. **94**, 152 (1983).

[284]M. Nakajima, Y. Sumiyoshi, and Y. Endo, Chem. Phys. Lett. **351**, 359 (2002).

[285]N. Reilly, G. Cupitt, S. Kable, and T. Schmidt, J. Chem. Phys. **124**, 194310 (2006).

[286]M. Nakajima, Y. Sumiyoshi, and Y. Endo, Chem. Phys. Lett. **355**, 116 (2002).

[287]H. Harjanto, W. W. Harper, and D. J. Clouthier, J. Chem. Phys. **105**, 10189 (1996).

[288]P. Ho, W. G. Breiland, and R. W. Carr, Chem. Phys. Lett. **132**, 422 (1986).

[289]R. de Nalda, A. Mavromanolakis, S. Couris, and M. Castillejo, Chem. Phys. Lett. **316**, 449 (2000).

[290]W. W. Harper and D. J. Clouthier, J. Chem. Phys. **106**, 9461 (1997).

[291]C. J. Evans and M. R. Dover, J. Phys. Chem. A **113**, 8533 (2009).

[292]M. R. Dover, C. J. Evans, and C. M. Western, J. Chem. Phys. **131**, 124302 (2009).

[293]Y.-Y. Lee, Y.-P. Lee, and N. S. Wang, J. Chem. Phys. **100**, 387 (1994).

[294]M. Kawasaki, "Laser-induced fluorescence of unstable intermediates in combustion: HSO and H$_2$CS," in *Laser Diagnostics and Modeling of Combustion*, edited by K. Iinuma, T. Ohsawa, T. Asanuma, and J. Doi (Springer, Berlin, Heidelberg, 1987), pp. 203–210.

[295]T. Yoshikawa, A. Watanabe, Y. Sumiyoshi, and Y. Endo, J. Mol. Spectrosc. **254**, 119 (2009).

[296]G. Rothschopf, T. C. Smith, and D. J. Clouthier, J. Chem. Phys. **156**, 184307 (2022).

[297]W. Lempert, G. Diskin, V. Kumar, I. Glesk, and R. Miles, Opt. Lett. **16**, 660 (1991).

[298]F. Northrup, J. Polanyi, S. Wallace, and J. Williamson, Chem. Phys. Lett. **105**, 34 (1984).

[299]T. Mosbach, H.-M. Katsch, and H. Döbele, Phys. Rev. Lett. **85**, 3420 (2000).

[300]O. Gabriel, D. Schram, and R. Engeln, Phys. Rev. E **78**, 016407 (2008).

[301]A. A. Turnipseed, M. K. Gilles, J. B. Burkholder, and A. Ravishankara, Chem. Phys. Lett. **242**, 427 (1995).

[302]W. J. Bloss, T. J. Gravestock, D. E. Heard, T. Ingham, G. P. Johnson, and J. D. Lee, J. Environ. Monit. **5**, 21 (2003).

[303]B. Hiller and R. Hanson, Exp. Fluids **10**, 1 (1990).

[304]S. Ezekiel and R. Weiss, Phys. Rev. Lett. **20**, 91 (1968).

[305]M. Zucco, L. Robertsson, and J. Wallerand, Metrologia **50**, 402 (2013).

[306]K.-C. Lin and H.-C. Chang, J. Chem. Phys. **90**, 6151 (1989).

[307]W. J. Tango, J. K. Link, and R. N. Zare, J. Chem. Phys. **49**, 4264 (1968).

[308]S. Milosevic, P. Kowalczyk, and G. Pichler, J. Phys. B: At. Mol. Phys. **20**, 2231 (1987).

[309]K. Meiwes and F. Engelke, Chem. Phys. Lett. **85**, 409 (1982).

[310]A. Ross, C. Effantin, J. d'Incan, and R. Barrow, J. Phys. B: At. Mol. Phys. **19**, 1449 (1986).

[311]T. Yoshikawa, Y. Sumiyoshi, H. Takada, K. Hoshina, and Y. Endo, J. Chem. Phys. **128**, 204308 (2008).

[312]M. Nakajima, Y. Yoneda, Y. Sumiyoshi, and Y. Endo, J. Chem. Phys. **120**, 2662 (2004).

[313]R. Heidner III, H. Helvajian, J. Holloway, and J. B. Koffend, J. Phys. Chem. **93**, 7813 (1989).

[314]U. Westblom and M. Alden, Appl. Spectrosc. **44**, 881 (1990).

[315]R. Beaman, T. Nelson, D. Richards, and D. Setser, J. Phys. Chem. **91**, 6090 (1987).

[316]A. Wodtke, L. Huwel, H. Schluter, G. Meijer, P. Andersen, and H. Voges, Opt. Lett. **13**, 910 (1988).

[317]A. Delon and R. Jost, J. Chem. Phys. **95**, 5686 (1991).

[318]J. B. Jeffries and D. R. Crosley, Combust. Flame **64**, 55 (1986).

[319]A. P. Ongstad, R. I. Lawconnell, and T. L. Henshaw, J. Chem. Phys. **97**, 1053 (1992).

[320]C. Zhu, H. Wang, B. Chen, Y. Chen, T. Yang, J. Yin, and J. Liu, J. Chem. Phys. **157**, 084307 (2022).

[321]B. Chen, Y.-N. Chen, J.-N. Pan, J.-P. Yin, and H.-L. Wang, Chin. Phys. B **31**, 093301 (2022).

[322]O. Shestakov, A. Pravilov, H. Demes, and E. Fink, Chem. Phys. **165**, 415 (1992).

[323]Y. Chen, Q. Zhang, D. Zhang, C. Chen, S. Yu, and X. Ma, Chem. Phys. Lett. **223**, 104 (1994).

[324]R. E. Huie, N. J. Long, and B. A. Thrush, J. Chem. Soc., Faraday Trans. 2 **74**, 1253 (1978).

[325]C. N. Xuan and A. Margani, J. Chem. Phys. **93**, 136 (1990).

[326]M. A. Clyne and M. C. Heaven, Chem. Phys. **58**, 145 (1981).

[327]K. N. Wong, W. R. Anderson, and A. J. Kotlar, J. Chem. Phys. **85**, 2406 (1986).

[328]N. Wang, Y. Ng, and A.-C. Cheung, Chem. Phys. Lett. **547**, 21 (2012).

[329]R. S. DaBell, R. G. Meyer, and M. D. Morse, J. Chem. Phys. **114**, 2938 (2001).

[330]T. C. Steimle and W. Virgo, J. Chem. Phys. **119**, 12965 (2003).

[331]C. Cheng, K. Guinn, I. Herman, and V. Donnelly, J. Vac. Sci. Technol., A **13**, 1970 (1995).

[332]T. C. Smith, H. Li, D. J. Clouthier, C. T. Kingston, and A. J. Merer, J. Chem. Phys. **112**, 3662 (2000).

[333]M. Suzuki, N. Washida, and G. Inoue, Chem. Phys. Lett. **131**, 24 (1986).

[334]Y. Nozaki, K. Kongo, T. Miyazaki, M. Kitazoe, K. Horii, H. Umemoto, A. Masuda, and H. Matsumura, J. Appl. Phys. **88**, 5437 (2000).

[335]M. Hertl, N. Dorval, O. Leroy, J. Jolly, and M. Péalat, Plasma Sources Sci. Technol. **7**, 130 (1998).

[336]Y. Matsumi, T. Hayashi, H. Yoshikawa, and S. Komiya, J. Vac. Sci. Technol., A **4**, 1786 (1986).

[337]M. Hertl and J. Jolly, J. Phys. D: Appl. Phys. **33**, 381 (2000).

[338]A. Kono, N. Koike, K. Okuda, and T. G. T. Goto, Jpn. J. Appl. Phys. **32**, L543 (1993).

[339]A. Kono, N. Koike, H. Nomura, and T. G. T. Goto, Jpn. J. Appl. Phys. **34**, 307 (1995).

[340]K. Greenberg and P. Hargis, Jr., J. Appl. Phys. **68**, 505 (1990).

[341]W. Weng, M. Alden, and Z. Li, Anal. Chem. **91**, 10849 (2019).

[342]A. L. Smith and J. B. Hopkins, J. Chem. Phys. **75**, 2080 (1981).

[343]Q. Zhang, P. Dupré, B. Grzybowski, and P. H. Vaccaro, J. Chem. Phys. **103**, 67 (1995).

[344]S. Nakhate, S. Mukund, and S. Bhattacharyya, J. Mol. Struct. **1243**, 130888 (2021).

[345]Z. Zhang, J. Guo, X. Yu, J. Zhen, and Y. Chen, J. Mol. Spectrosc. **253**, 112 (2009).

[346]N. Zhao, D. Lei, X. Li, J. Li, Q. Ma, Q. Zhang, L. Guo, and Y. Lu, Appl. Opt. **58**, 1895 (2019).

[347]R. Dreyfus, R. Kelly, and R. Walkup, Appl. Phys. Lett. **49**, 1478 (1986).

[348]G. S. Selwyn, Appl. Phys. Lett. **51**, 167 (1987).

[349]C. Li, Z. Hao, Z. Zou, R. Zhou, J. Li, L. Guo, X. Li, Y. Lu, and X. Zeng, Opt. Express **24**, 7850 (2016).

[350]X. Aubert, C. Duluard, N. Sadeghi, and A. Gicquel, Plasma Sources Sci. Technol. **26**, 115011 (2017).

[351]N. Sirse, M. Foucher, P. Chabert, and J.-P. Booth, Plasma Sources Sci. Technol. **23**, 062003 (2014).

[352]M. Aldén, P.-E. Bengtsson, and U. Westblom, Opt. Commun. **71**, 263 (1989).

[353]J. Booth, Y. Azamoum, N. Sirse, and P. Chabert, J. Phys. D: Appl. Phys. **45**, 195201 (2012).

[354]M. Heaven, T. A. Miller, R. R. Freeman, J. White, and J. Bokor, Chem. Phys. Lett. **86**, 458 (1982).

[355]W. Sdorra, A. Quentmeier, and K. Niemax, Microchim. Acta **98**, 201 (1989).

[356]B. Gellert, J. Phys. D: Appl. Phys. **21**, 710 (1988).

03 December 2024 20:43:44

[357]J. Gao, N. Nafarizal, and K. Sasaki, J. Vac. Sci. Technol., A **24**, 2100 (2006).

[358]M. Bolshov, A. Zybin, and I. Smirenkina, Spectrochim. Acta, Part B **36**, 1143 (1981).

[359]H. Falk, H.-J. Paetzold, K. Schmidt, and J. Tilch, Spectrochimica Acta, Part B **43**, 1101 (1988).

[360]C. Hecht, H. Kronemayer, T. Dreier, H. Wiggers, and C. Schulz, Appl. Phys. B **94**, 119 (2009).

[361]W. Ma, S. Tao, D. Zhang, and D. Chen, Anal. Sci. **17**, a215 (2002).

[362]P. Brewer, P. Das, G. Ondrey, and R. Bersohn, J. Chem. Phys. **79**, 720 (1983).

[363]K. Zhu, S. J. Barkley, C. E. Dedic, T. R. Sippel, and J. B. Michael, Appl. Opt. **59**, 5632 (2020).

[364]J. W. Daily and C. Chan, Combust. Flame **33**, 47 (1978).

[365]T. Erdmann, H. Figger, and H. Walther, Opt. Commun. **6**, 166 (1972).

[366]S. Laville, C. Goueguel, H. Loudyi, F. Vidal, M. Chaker, and M. Sabsabi, Spectrochim. Acta, Part B **64**, 347 (2009).

[367]P. Brewer, N. Van Veen, and R. Bersohn, Chem. Phys. Lett. **91**, 126 (1982).

[368]R. Roth, K. Spears, and G. Wong, Appl. Phys. Lett. **45**, 28 (1984).

[369]N. Britun, M. Gaillard, and J. Han, J. Phys. D: Appl. Phys. **41**, 185201 (2008).

[370]T. Lunt, G. Fussmann, and O. Waldmann, Phys. Rev. Lett. **100**, 175004 (2008).

[371]Y. Tanida, D. Kuwahara, and S. Shinohara, Trans. Jpn. Soc. Aeronaut. Space Sci. Aerosp. Technol. Jpn. **14**, 7 (2016).

[372]S. C. Thakur, J. Gosselin, J. McKee, E. Scime, S. Sears, and G. Tynan, Phys. Plasmas **23**, 082112 (2016).

[373]C. Biloiu, X. Sun, E. Choueiri, F. Doss, E. Scime, J. Heard, R. Spektor, and D. Ventura, Plasma Sources Sci. Technol. **14**, 766 (2005).

[374]G. Severn, X. Wang, E. Ko, N. Hershkowitz, M. Turner, and R. McWilliams, Thin Solid Films **506**, 674 (2006).

[375]T. Bieber, S. Bardin, L. De Poucques, R. Brochard, R. Hugon, J. Vasseur, and J. Bougdira, Plasma Sources Sci. Technol. **20**, 015023 (2011).

[376]A. M. Keesee, E. E. Scime, and R. F. Boivin, Rev. Sci. Instrum. **75**, 4091 (2004).

[377]D. Kuwahara, Y. Tanida, M. Watanabe, N. Teshigahara, Y. Yamagata, and S. Shinohara, Plasma Fusion Res. **10**, 3401057 (2015).

[378]G. Severn, D. Edrich, and R. McWilliams, Rev. Sci. Instrum. **69**, 10 (1998).

[379]S. K. S. Kumagai, M. S. M. Sasaki, M. K. M. Koyanagi, and K. H. K. Hane, Jpn. J. Appl. Phys. **38**, 7126 (1999).

[380]M. Malyshev, N. Fuller, K. Bogart, V. Donnelly, and I. P. Herman, Appl. Phys. Lett. **74**, 1666 (1999).

[381]C.-C. Zen and Y.-P. Lee, Chem. Phys. Lett. **244**, 177 (1995).

[382]M. Nakajima, Y. Yoneda, Y. Sumiyoshi, T. Nagata, and Y. Endo, J. Chem. Phys. **119**, 7805 (2003).

[383]T. E. Steinberger and E. E. Scime, J. Propul. Power **34**, 1235 (2018).

[384]A. Lejeune, G. Bourgeois, and S. Mazouffre, Phys. Plasmas **19**, 073501 (2012).

[385]W. Hargus, G. M. Azarnia, and M. R. Nakles, "Demonstration of laser-induced fluorescence on a krypton hall effect thruster," paper presented at the 32nd International Electric Propulsion Conference, 11–15 September 2011, Wiesbaden, Germany.

[386]M. Tremblay, B. W. Smith, and J. D. Winefordner, Anal. Chim. Acta **199**, 111 (1987).

[387]B. Woodcock, J. Busby, T. Freegarde, and G. Hancock, J. Appl. Phys. **81**, 5945 (1997).

[388]Y. Matsuo, T. Nakajima, T. Kobayashi, and M. Takami, Appl. Phys. Lett. **71**, 996 (1997).

[389]T. Smith, B. Ngom, J. Linnell, and A. Gallimore, "Diode laser-induced fluorescence of xenon ion velocity distributions," in *41st AIAA/ASME/SAE/ASEE Joint Propulsion Conference & Exhibit*, Tucson, Arizona, 10–13 July 2005 (AIAA, 2005), p. 4406.

[390]T. Smith, D. Herman, A. Gallimore, and G. Williams, "Laser-induced fluorescence velocimetry of Xe II in the 30-cm NSTAR-type ion engine plume," in *40th AIAA/ASME/SAE/ASEE Joint Propulsion Conference and Exhibit*, Fort Lauderdale, Florida, 11–14 July 2004 (AIAA, 2004), p. 3963.

[391]N. Sadeghi, M. Van De Grift, D. Vender, G. Kroesen, and F. De Hoog, Appl. Phys. Lett. **70**, 835 (1997).

[392]R. Engeln, S. Mazouffre, P. Vankan, D. Schram, and N. Sadeghi, Plasma Sources Sci. Technol. **10**, 595 (2001).

[393]Z. D. Short, M. U. Siddiqui, M. F. Henriquez, J. S. McKee, and E. E. Scime, Rev. Sci. Instrum. **87**, 013505 (2016).

[394]R. Bergert, L. W. Isberner, S. Mitic, and M. H. Thoma, Phys. Plasmas **28**, 013301 (2021).

[395]S. Hansen, G. Luckman, G. C. Nieman, and S. D. Colson, Appl. Phys. Lett. **56**, 719 (1990).

[396]M. J. Frost, S. Himmelmann, and D. Palmer, J. Phys. B: At., Mol. Opt. Phys. **34**, 1569 (2001).

[397]W. Rellergert, S. Cahn, A. Garvan, J. Hanson, W. Lippincott, J. Nikkel, and D. McKinsey, Phys. Rev. Lett. **100**, 025301 (2008).

[398]W. Hargus, "A preliminary study of krypton laser-induced fluorescence," in *46th AIAA/ASME/SAE/ASEE Joint Propulsion Conference & Exhibit*, Nashville, TN, 25–28 July 2010 (AIAA, 2010), p. 6524.

[399]M. Mustafa, M. B. Hunt, N. J. Parziale, M. S. Smith, and E. C. Marineau, "Krypton tagging velocimetry (KTV) investigation of shock-wave/turbulent boundary-layer interaction," in *55th AIAA Aerospace Sciences Meeting*, Grapevine, Texas, 9–13 January 2017 (AIAA, 2017), p. 0025.

[400]S. Nemschokmichal, F. Bernhardt, B. Krames, and J. Meichsner, J. Phys. D: Appl. Phys. **44**, 205201 (2011).

[401]R. Ono, C. Tobaru, Y. Teramoto, and T. Oda, Plasma Sources Sci. Technol. **18**, 025006 (2009).

[402]X. Shen, H. Wang, Z. Xie, Y. Gao, H. Ling, and Y. Lu, Appl. Opt. **48**, 2551 (2009).

[403]H. Kondo, N. Hamada, and K. Wagatsuma, Spectrochim. Acta, Part B **64**, 884 (2009).

[404]S. Mazouffre, G. Bourgeois, L. Garrigues, and E. Pawelec, J. Phys. D: Appl. Phys. **44**, 105203 (2011).

[405]R. Cedolin, W. Hargus, Jr., P. Storm, R. Hanson, and M. Cappelli, Appl. Phys. B **65**, 459 (1997).

[406]G. S. Oehrlein *et al.*, J. Vac. Sci. Technol. B **42**, 041501 (2024)